Hydrogeology Journal (2015) 23: 175–194
DOI 10.1007/s10040-014-1188-z

Analysis of groundwater dynamics in the complex aquifer system of Kazan Trona, Turkey, using environmental tracers and noble gases

Sebnem Arslan · Hasan Yazicigil · Martin Stute · Peter Schlosser · William M. Smethie, Jr.

Abstract The Eocene deposits of Kazan Basin in Turkey contain a rare trona mineral which is planned to be extracted by solution mining. The complex flow dynamics and mixing mechanisms as noted from previous hydraulic and hydrochemical data need to be augmented with environmental tracer and noble gas data to develop a conceptual model of the system for the assessment of the impacts of the mining and to develop sustainable groundwater management policies throughout the area. The tracers used include the stable isotopes of water (δ^2H, δ^{18}O), δ^{13}C and ^{14}C of dissolved inorganic carbon (DIC), tritium (^{3}H), the chlorofluorocarbons CFC-11 and CFC-12, and the noble gases He and Ne. The system studied consists of three aquifers: shallow, middle, and deep. CFC data indicate modern recharge in the shallow system. The estimates of ages through ^{14}C dating for the deeper aquifer system are up to 34,000 years. Helium concentrations cover a wide range of values from 5×10^{-8} to 1.5×10^{-5} cm^3 STP/g. ^{3}He/^{4}He ratios vary from $0.09R_A$ to $1.29R_A$ (where R_A is the atmospheric ^{3}He/^{4}He ratio of 1.384×10^{-6}), the highest found in water from the shallow aquifer. Mantle-derived ^{3}He is present in some of the samples indicating upward groundwater movement, possibly along a NE–SW-striking fault-like feature in the basin.

Keywords Turkey · Groundwater age · Complex aquifer system · Stable isotopes · Helium isotopes

Received: 17 December 2013 / Accepted: 28 August 2014
Published online: 17 September 2014

S. Arslan · H. Yazicigil
Department of Geological Engineering,
Middle East Technical University, 06800, Ankara, Turkey

S. Arslan · M. Stute · P. Schlosser · W. M. Smethie
Lamont-Doherty Earth Observatory of Columbia University,
Palisades, NY 10964, USA

S. Arslan
Faculty of Engineering Department of Geological Engineering,
Ankara University, Tandogan, 06100, Ankara, Turkey

M. Stute
Department of Environmental Science,
Barnard College, New York, NY 10027, USA

P. Schlosser
Department of Earth and Environmental Sciences,
Columbia University, New York, NY 10027, USA

P. Schlosser
Department of Earth and Environmental Engineering,
Columbia University, New York, NY 10027, USA

S. Arslan (✉)
Faculty of Engineering Department of Geological Engineering,
Ankara University, Tandogan, 06100, Ankara, Turkey
e-mail: sebnem_okten@yahoo.com
Tel.: +90 312 2033416

Introduction

Proper understanding of the hydrogeological setting and development of a conceptual model are prerequisites for a reliable assessment of the impacts of solution mining and other activities on groundwater systems. Although the hydraulic and chemical data from monitoring wells provide a reliable estimate of the conceptual model for simple systems, it is often necessary to have additional data for those systems that involve complex flow patterns and mixing conditions. In recent decades, environmental tracers have been used in numerous studies of complex groundwater flow systems (e.g., Szabo et al. 1996; Clark et al. 1997; Castro et al. 2000; and many others). Such studies included determination of groundwater residence times (e.g., Schlosser et al. 1988, 1989; Stute and Deak 1989; Stute et al. 1992a; Busenberg and Plummer 1992; Aeschbach-Hertig et al. 1998; Busenberg and Plummer 2000; among others), recharge rates and dispersion (e.g., Robertson and Cherry 1989; Solomon and Sudicky 1991), calculation of groundwater velocity, or identification of subsurface processes affecting the quality of groundwater (Clark and Fritz 1997). Groundwater age is usually used to define the amount of time passed between recharge of a water parcel at the water table and sampling at a well or natural discharge point (Newman et al. 2010). Any groundwater parcel is a mixture of waters which resided in the saturated zone for different intervals of time and the age of the sample calculated by a dating method is affected by this mixing (e.g., Bethke and Johnson 2008). For example, the age of a mixture predicted by asymptotic

decay methods might be biased towards younger ages if the mixture contains both young and very old components (Weissmann et al. 2002; Bethke and Johnson 2008). Busenberg and Plummer (1992), Varni and Carrera (1998) and Weissmann et al. (2002) emphasized that subsurface heterogeneity and groundwater mixing due to hydrodynamic dispersion influence tracer-based ages and produce uncertainty in estimates of mean groundwater ages. Newman et al. (2010) suggest that in fractured rock systems, considerable discrepancies between apparent groundwater ages are obtained using different tracers. These discrepancies might be due to mixing of water with different ages. The mixing between young and old groundwater was recently studied by Solomon et al. 2010; Samborska et al. 2013, and Yager et al. 2013. Yager et al. (2013) simulated flow in a karst aquifer flowing mainly through fractured zones. In this study, the numerical model exhibited a flow field including recently recharged younger water traveling through a complex set of shallow flow paths mixing with older water traveling along fault zones. According to Solomon et al. (2010), Sanford (2011), Eberts et al. (2012) and Yager et al. (2013), the uncertainty in estimated parameter values was decreased when environmental tracer concentrations were included in groundwater flow models. Furthermore, helium accumulation in groundwater has been studied in many parts of the world by various researchers and crustal and mantle ^{4}He fluxes were successfully established (Martel et al. 1989; Stute et al. 1992b; Castro et al. 2000; Kulongoski et al. 2003; and many others) to provide information on mixing processes.

After the discovery of a trona ore deposit in Eocene formations of the Kazan Basin 35 km northwest of Ankara (Fig. 1), detailed hydrogeological and hydrogeochemical characterizations were carried out to assess the potential impacts of solution mining on groundwater resources (SRK 2001, 2004; Yazicigil et al. 2001, 2009; Arslan 2008; Camur et al. 2008). Water resources are very important for the local community since the area is located in a semi-arid climate in Central Anatolia.

Trona mineral is chemically known as sodium sesquicarbonate ($Na_2CO_3.NaHCO_3.2H_2O$) and is refined to soda ash by means of dissolution and recrystallization. Soda ash is an inorganic chemical used for manufacturing of glass, paper, laundry detergents and many other products and chemicals, including baking soda. Although trona is a rare mineral throughout the world, there are two deposits in Turkey. The discovery of the first Turkish trona deposit was made by the General Directorate of Mineral Research and Exploration in 1982 in the Beypazari Basin, whereas the second one was made by Rio Tinto in 1998 in the Eocene deposits of the Kazan basin. There are plans for extraction of the Kazan trona deposit. Such extraction has to be done by solution mining because of its depth and low-grade. Solution mining method would require the injection of hot, pressurized water through a vertical injection hole which is connected to a 500-m-long horizontal well drilled along the base of the trona. Trona would be dissolved by the injected fluid and a production fluid would then be recovered through a vertical production well connected to the end of the horizontal well. The quantity of water required for the mining facility is estimated to be as high as 100 l/s (3.2×10^6 m^3/year; SRK 2003). This quantity of water is significant and is almost equal to the current drinking and domestic water use of the 42,000 people residing in the basin. Thus, it is vital to have information on the groundwater residence times throughout the area to enhance the hydrogeological understanding and conceptual model of groundwater flow to reliably assess the impacts of solution mining of trona on groundwater resources and to plan sustainable groundwater management strategies minimizing the effects of water use by mining.

The rock formations present in Kazan Basin were studied by Kocyigit and Lunel (1987), Kazanci and Gokten (1988), and Kocyigit et al. (1988). A detailed geological investigation of the study area was carried out by Toprak and Rojay (2000, 2001), and Rojay et al. (2002). In this system, the significant water-bearing units are found in shallow (Plio-Quaternary), middle (Neogene) and deep (Eocene) groundwater systems. The initial hydrogeological studies conducted in the Kazan Basin date back to the 1970s (DSI 1975); however, detailed hydrogeological investigations started only after the discovery of the trona deposit in 1998. These studies, concentrated in the deposit area, aimed at characterizing the groundwater resources in the area (SRK 2001, 2004; Yazicigil et al. 2001; Camur et al. 2008). These previous studies based on hydraulic and hydrochemical data have been unable to characterize the flow and mixing processes in detail. In a recent study, Arslan et al. (2013) discussed climate change from the late Pleistocene to the Holocene by using environmental isotopes ($\delta^{18}O$, $\delta^{2}H$, $\delta^{13}C$, ^{14}C) and noble gas thermometry. They concentrated on the tracer data obtained from the deep groundwater system and used the data from the shallow aquifer only to compare modern recharge conditions to those in the past. Noble gas and radiocarbon data were examined in detail, recharge temperatures were obtained through inverse modeling calculations and radiocarbon ages were acquired by using a $\delta^{13}C$ correction model (Arslan et al. 2013). The study provided paleotemperature information for central Turkey, particularly around Ankara, where no information on late Pleistocene climate was available. The mixing mechanisms between different aquifers and the groundwater dynamics in the area were beyond the scope of Arslan et al. (2013) and are addressed in this contribution. In particular, the presence or absence of a suspected NE–SW striking fault passing through about 1 km southeast of the deposit area would have a significant effect on the dynamics of the groundwater flow and the mixing observed. Additionally, the large discrepancy noted in the calculated hydraulic ages demonstrated the need to use tracer techniques for estimates of more reliable residence times throughout the study area (Arslan 2008). This study was undertaken

 DOI 10.1007/s10040-014-1188-z

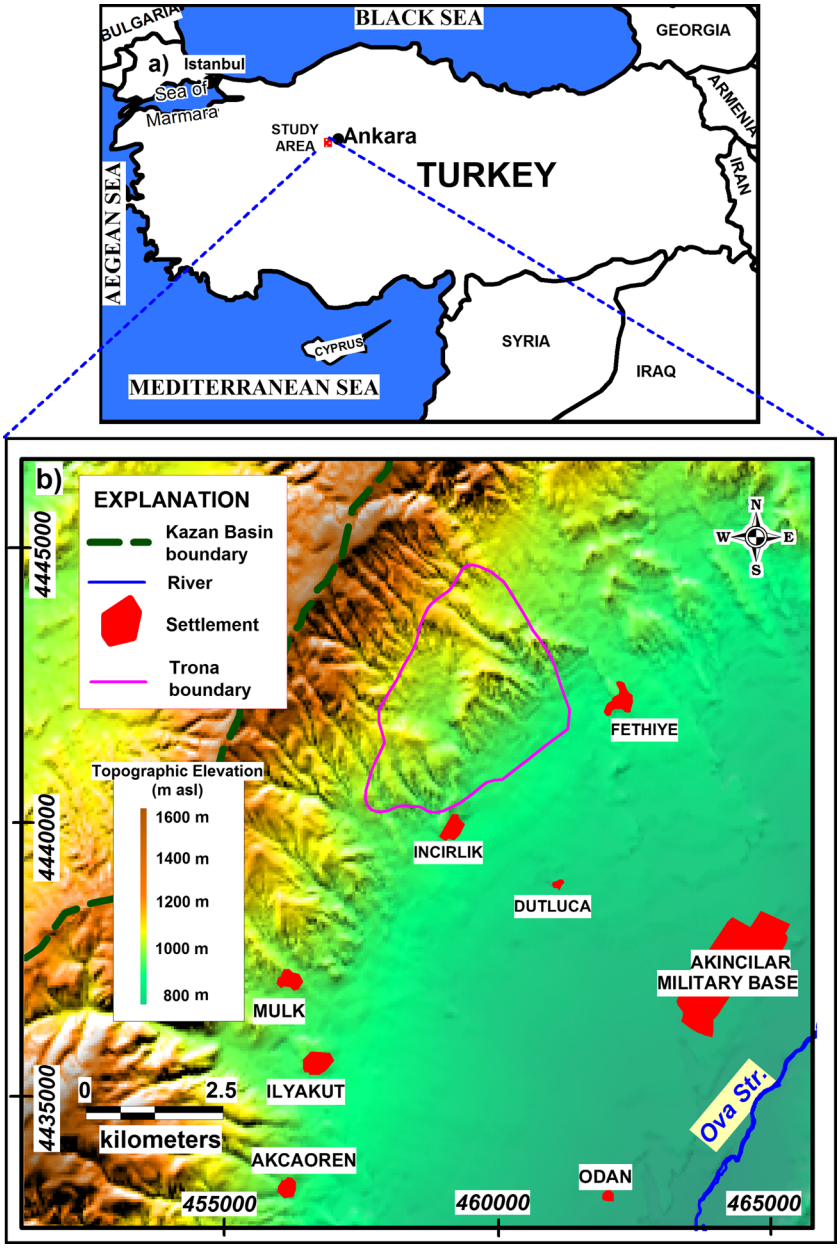

Fig. 1 **a** Location and **b** relief maps of the study area

with the purpose of determining the mean groundwater residence times and the mixing processes between the aquifers of the complex system located above the Kazan trona ore field by using environmental tracers including $\delta^{18}O$, $\delta^{2}H$, $\delta^{13}C$, ^{14}C, CFC-11, CFC-12 and dissolved noble gases. The ultimate goal of the study is to provide input into the development of a conceptual hydrogeological model that will enhance the hydrogeological understanding of the complex aquifer system. A numerical groundwater flow model can then be developed to better assess the impacts of solution mining of trona on groundwater resources and to plan sustainable groundwater management policies to mitigate the effects of solution mining and its water use.

Study area description

Geographical setting and climate

The study area is located 35 km northwest of Ankara, Turkey, on the flanks of the Kazan Basin, which is an elongated NE–SW trending depression with an average width of 10 km and a length of 40–45 km (Fig. 1). In the basin, there are two morphologically distinct formations: a plain and a mountainous region. The flat part is called the Murted Plain, an elevated plateau that ranges in elevation from 950 m above sea level (masl) in the north to about 800 masl in the south with an average elevation of 875 m. The highest elevation in the mountainous region is 1,408 m decreasing gradually to 850 m toward the southeast (Fig. 1).

DOI 10.1007/s10040-014-1188-z

The study area, located in Central Anatolia, has a continental semi-arid climate with moderate to hot, dry summers and moist, cold winters. The average annual mean temperature, precipitation, and potential evapotranspiration recorded at Ankara Station between 1930 and 2006 are 11.8 °C, 389.1 mm, and 1112.2 mm, respectively.

Geology of the study area

The Kazan Basin is one of the several neotectonic depressions in central Turkey. According to the geological studies carried out by Toprak and Rojay (2000, 2001) and Rojay et al. (2002), four rock sequences are exposed in the study area which are Paleozoic metamorphics, Eocene units (Mulk and Akpinar Formations), Neogene Units and Plio-Quaternary deposits (Figs. 2 and 3). Paleozoic metamorphics are the basement rocks in the area and they are composed of graphitic schists enclosing intensely fractured and recrystallized limestones. Eocene units deposited conformably on the basement units and are developed as the transgressive sequence from a lacustrine to a shallow marine environment. The Eocene Mulk Formation is the lower sequence hosting the trona deposit and consists of siltstones-sandstones, alternating marls, clayey limestones and organic-rich dolomitic mudstone beds. The Mulk Formation is divided into four lithostratigraphic sequences: Incirlik member, clastic wedge, Asmalidere member and Fethiye member (Fig. 2). The upper Akpinar Formation is unconformably overlain by the Neogene units and it also has a conformable contact with Fethiye member. It consists of siltstones-sandstones and marls followed by limestones. The lower sequence of Neogene units, located in the northwestern part of the area, is composed of fractured clayey and cherty limestones and mudstones. The upper sequence consists of conglomerates at the northwest of Fethiye village and mudstone, sandstone and conglomerates followed by limestones and tuffaceous clastics around northwest of Incirlik village. The Pliocene units, deposited unconformably on the Neogene units, are composed of conglomerates and sandstone-siltstone-mudstone alternations. The Quaternary deposits consist of alluvium, alluvial fans and slope deposits and the colluvium/talus accumulations (Toprak and Rojay 2000).

Hydrogeologic setting

Hydrogeologic classification of the various units in the study area was done by Yazicigil et al. (2009) using 58 wells monitoring different depths ranging from 7 to 850 m below ground surface. The water-bearing units within the study area are the alluvium and the porous and fractured zones of the Neogene and Eocene lacustrine units. These units form three different aquifers identified as shallow, middle and deep (Fig. 4).

Shallow groundwater system

The shallow aquifer system occurs as a regional aquifer under unconfined conditions in the Quaternary alluvial deposits. The uppermost weathered and fractured sections of the Neogene form a local perched aquifer that is part of

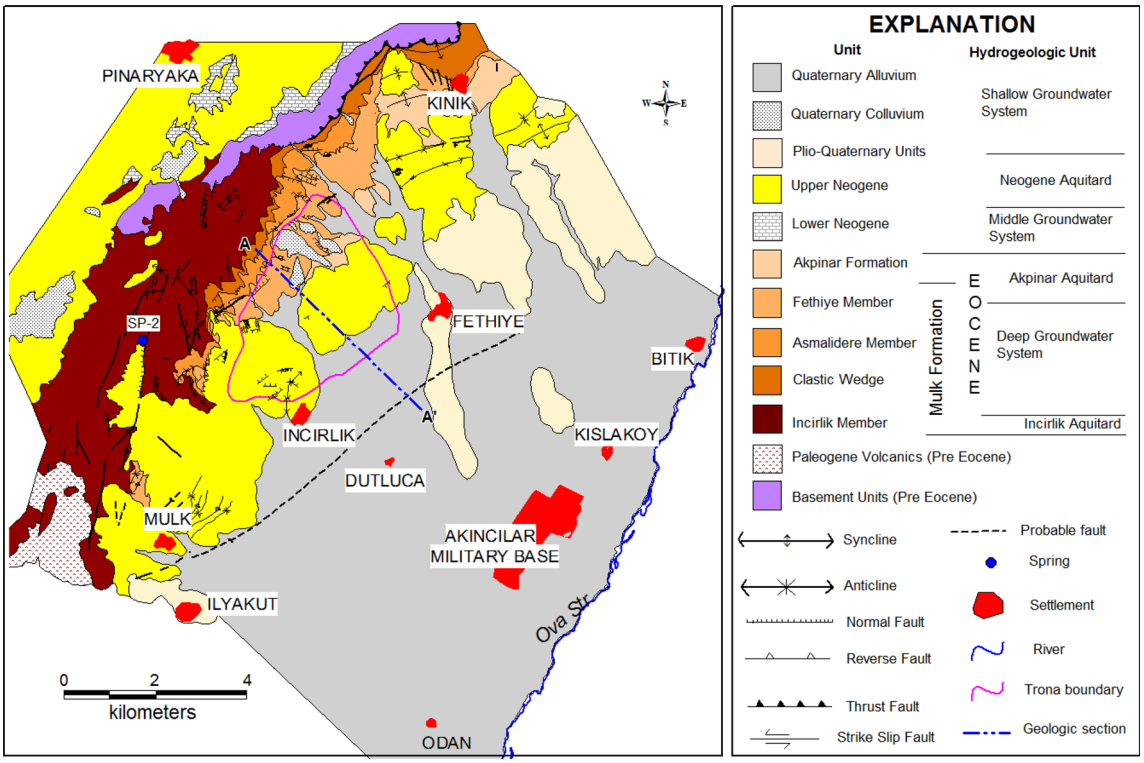

Fig. 2 Geological map of the study area (Modified from Toprak and Rojay 2001)

DOI 10.1007/s10040-014-1188-z

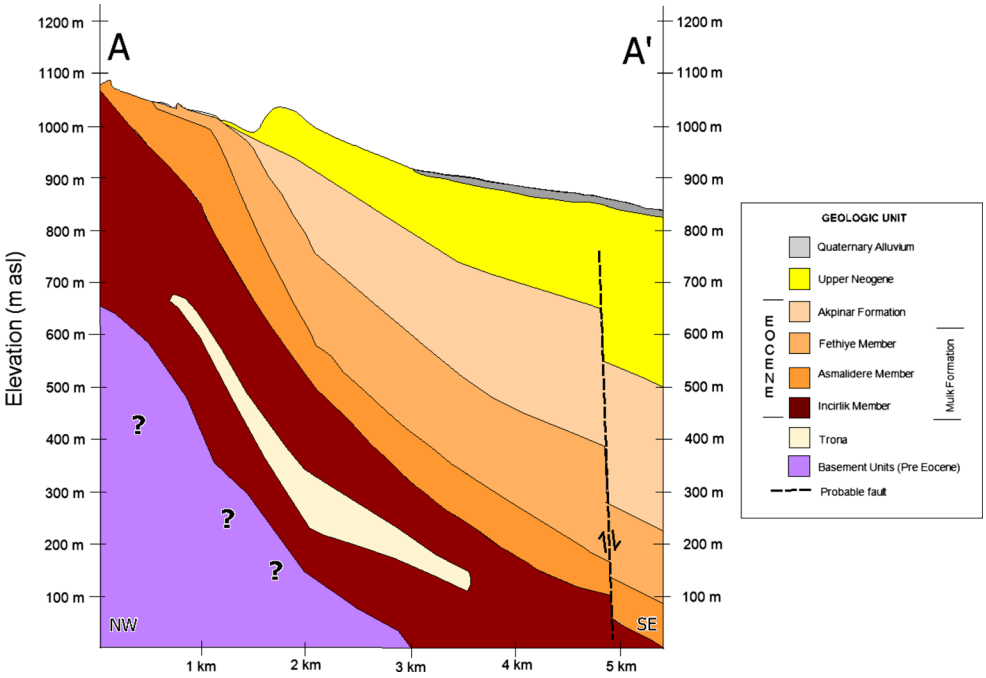

Fig. 3 Geological cross-section (See Fig. 2 for location)

the shallow system (Fig. 4). The thickness of the alluvium varies from a few meters to 15–20 m in the study area, increasing to 30–35 m along the Ova Stream in the east. The water-table contour map for the shallow aquifer for March 2003 shows that groundwater in the alluvium flows southeast toward the Ova Stream (Fig. 5). The hydraulic gradient is around 0.03 along the margins of the plain in the west and 0.007 in the southeast. In the alluvium, the depth to water table varies from 1 to 15 m (SRK 2004). Monthly monitoring data show groundwater levels rise during the wet season at monitoring wells S-1, S-2 and S-13, which are located in front of the mountain range at the edge of the basin (Fig. 5a). According to the results of slug tests performed by Yazicigil et al. (2009), the hydraulic conductivity of the alluvium ranges from 1×10^{-6} to 7.7×10^{-5} m/s, whereas the hydraulic conductivity in the shallow Neogene system ranges from 5.4×10^{-7} to 1×10^{-5} m/s. These results suggest that the uppermost Neogene is not as permeable as the alluvium.

Middle groundwater system

The middle groundwater system, unlike the shallow one, is under confined conditions except for outcrops and is present in the basal conglomerates of the Neogene unit and in the fractured network developed as a result of faulting (Fig. 4). Sloping downward towards the east, this system is exposed in the middle of the study area. The

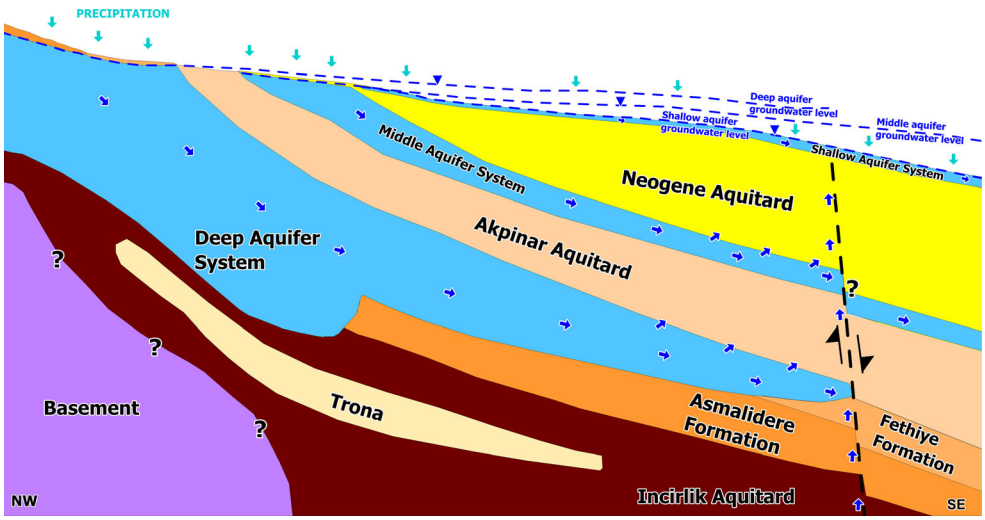

Fig. 4 Conceptual groundwater flow model of the study area

 DOI 10.1007/s10040-014-1188-z

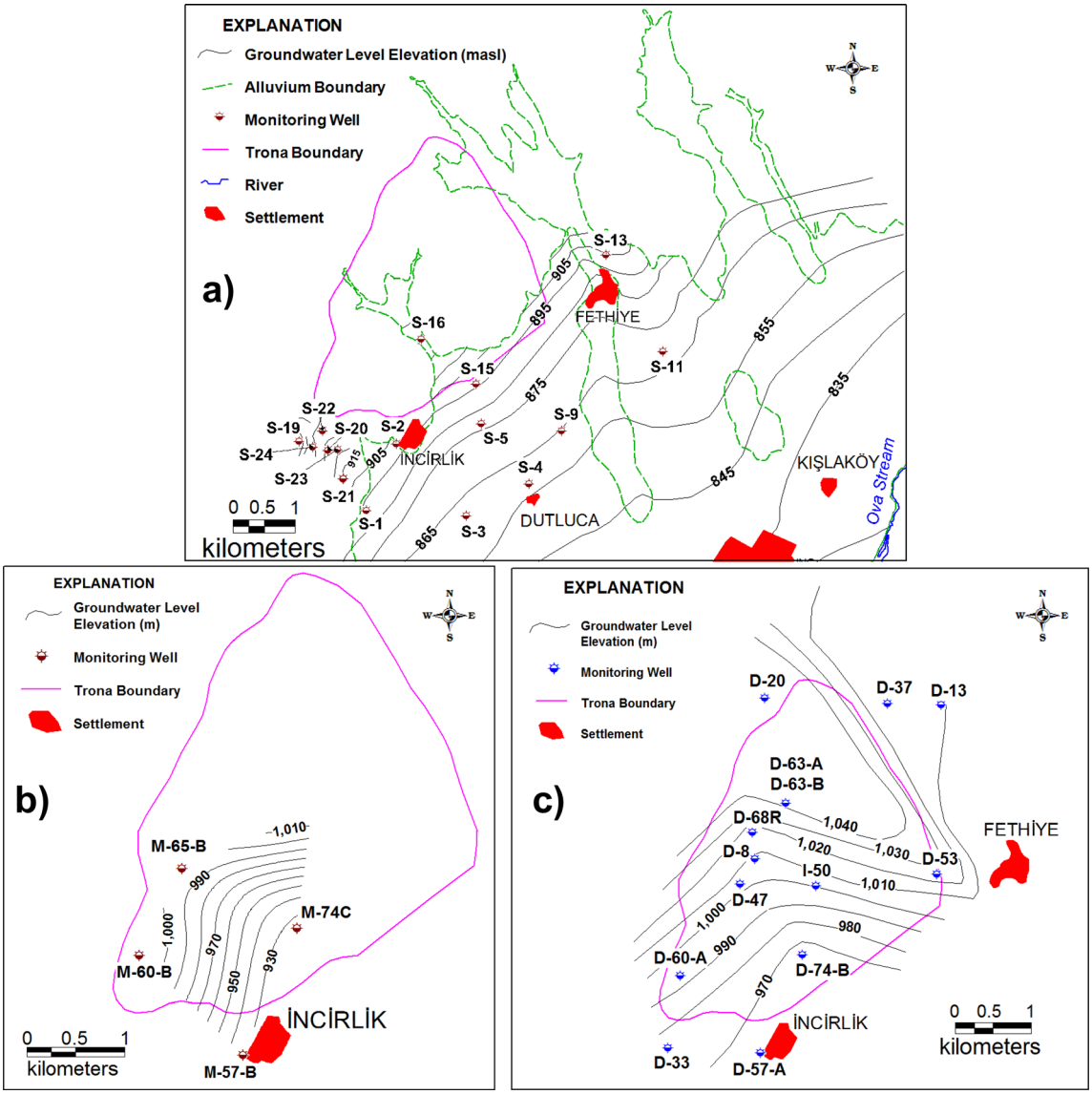

Fig. 5 Hydraulic head distribution maps for **a** shallow aquifer **b** middle aquifer and **c** deep aquifer, in March 2003 (SRK 2004)

groundwater flow is towards the SE in this system (Fig. 5b). The horizontal hydraulic gradients change between 0.07 and 0.1. The upward vertical gradient becomes evident (0.21) downstream near wells M-57B and M-74C. It is separated from the underlying deep aquifer by an aquitard (Akpinar Formation) in the north of İncirlik village. Toward the south of Incirlik village, it lies directly above the deep aquifer. The average thickness of this aquifer is about 50 m (SRK 2001). The hydraulic conductivity values for this system range from 9.4×10^{-6} to 4.9×10^{-8} m/s.

Deep groundwater system

The deep groundwater system is confined in the extensively fractured sections of the Eocene Mulk Formation (Fig. 4). There is a saline zone in this deep, fractured-rock system at the southern half of the trona deposit area with a considerable impact on groundwater quality (Camur et al. 2008). The thickness of this fractured aquifer exceeds 400 m to the west of the trona deposit area decreasing progressively towards east to about 100–150 m (SRK 2004). The system is mostly confined except in outcrop areas. The hydraulic head map for the deep aquifer shows a groundwater mound at the northern end of the trona deposit with groundwater flow to the south and northeast from this mound with a horizontal gradient of 0.04 (Fig. 5c). There is an upward vertical gradient between the deep aquifer system and overlying units as observed in the wells D-57-A and D-74-B with an increasing magnitude in the direction of flow to values as high as 0.25 (SRK 2004). The hydraulic conductivity values range from 2×10^{-10} m/s in the matrix rock at wells D-53 and D-13 to 3×10^{-4} m/s in the most fractured sections at wells D-33, D-47, D-63-A, D-63-B, D-8 and D-68R. Well locations are displayed in Fig. 5c.

DOI 10.1007/s10040-014-1188-z

The initial hydrogeological conceptual model of the Kazan Trona deposit area was developed by Yazicigil et al. (2009). They postulated that the deeper fractured aquifer system, having a greater potentiometric surface than the middle Neogene and the shallow alluvial system, sets up an upward gradient, thereby recharging them in downgradient areas where the deeper aquifer wedges out due to decreasing intensity of fractures. They considered that the wedging of the deep aquifer system toward the southeast of the area acts as a barrier to the groundwater flow and forces the flow upward. The likely existence of this upward movement of deep groundwater along a suspected buried fault that runs in NE–SW direction along the southeastern part of the study area was not taken into account in previous studies. The aim of this study is to test these hypotheses by using environmental isotopes and noble gases in order to enhance the understanding of the hydrogeological conditions and improve the existing conceptual model.

Methods

Sampling procedures

Between the summers of 2006 and 2007, three field trips were carried out and a total of 37 representative samples were collected from the Kazan Basin monitoring wells. Temperature, pH, electrical conductivity and dissolved oxygen were measured in the field (Table 1). The dissolved oxygen measurements were done by using a colorimetric method (CHEMet Kit, ASTM 1999; Gilbert et al. 1982). Water samples were collected after temperature, pH and electrical conductivity became constant to ensure that the samples were representative of the water in the aquifer. Samples for stable isotope analysis were collected in 60-ml Boston round clear glass bottles with 20-mm-sized screw caps. Samples for tritium, ^{13}C and ^{14}C were collected in 250-ml Boston round clear glass bottles with 24-mm screw caps. The ^{14}C samples were preserved by adding 0.2 ml of saturated $HgCl_2$ solution to prevent post-collection biological activity from altering the carbon

Table 1 Monitoring well and field chemical data

Sample	Depth to screened zone [m]		Aquifer	Coordinates		Cond. [μS/cm]	Temp. [C°]	pH	DO [mg/l]	Chemical character
	Top	Bottom		Northing	Easting					
S-1	8	20	SU	458389.7	4438691.6	475	13.0	7.88	5.0	Ca–Mg–HCO_3
S-2	8	20	SU	458866.8	4439755.7	742	13.4	7.94	2.0	Ca–Mg–HCO_3
S-3	8	20	SU	459986.4	4438608.1	726	14.3	7.53	3.0	Ca–Mg–HCO_3
S-4	5	9	SU	461000.0	4439113.0	14,069	15.2	7.64	0.7	Na–SO_4
S-5	8	20	SU	460231.6	4440080.6	625	13.9	7.96	10.0	Ca–Mg–HCO_3
S-9	7	15	SU	461520.5	4439964.2	2,673	13.6	8.32	0.1	Na–SO_4–Cl
S-11	4	12	SU	463142.2	4441246.7	816	14.6	7.71	0.4	Ca–Mg–HCO_3
S-13	4	12	SU	462230.8	4442793.2	642	14.3	7.80	ND	Ca–Mg–HCO_3
S-15	10	14	SU	460150.0	4440718.0	1,081	12.2	7.97	4.0	Ca–Mg–HCO_3
S-16	7	23	SU	459264.3	4441443.7	725	11.1	7.62	5.5	Ca–Mg–HCO_3
S-19	4	20	SNU	457306.5	4439795.9	610	13.3	7.90	5.0	Ca–Mg–HCO_3
S-20	4	20	SNU	457763.0	4439650.9	526	12.1	7.75	5.0	Ca–Mg–HCO_3
S-21	4	20	SNU	458023.7	4439202.8	434	13.0	7.84	ND	Ca–Mg–HCO_3
S-22A	13	21	SNU	457680.0	4439963.3	684	12.8	7.67	5.0	Ca–Mg–HCO_3
S-23	4	20	SNU	457920.9	4439664.4	504	11.7	7.69	5.0	Ca–Mg–HCO_3
S-24	4	20	SNU	457526.8	4439709.6	614	12.5	7.65	2.0	Ca–Mg–HCO_3
D-8	158.99	188.74	DC	458803.4	4442308.8	3,130	18.4	9.61	0.0	Na–HCO_3
D-13	361.79	391.54	DC	461261.3	4444346.2	920	13.5	8.91	0.0	Na–HCO_3
D-20	191.96	221.71	DC	458931.9	4444438.2	879	15.0	7.57	ND	Ca–Mg–HCO_3
D-33	151.43	163.33	DC	457656.3	4439808.0	1,759	15.7	8.74	0.0	Na–HCO_3
D-37	211.78	241.53	DC	460556.8	4444364.9	880	16.9	8.96	0.0	Na–HCO_3
D-47	72	372	DC	458608.2	4441977.3	5,486	17.2	9.24	0.05	Na–HCO_3
I-50	808.5	820.5	IA	459607.5	4441948.1	25,720	16.9	10.02	ND	Na–HCO_3
D-53	546	576	DC	461207.0	4442103.7	6,354	12.3	9.20	ND	Na–HCO_3
D-57A	300.71	318.62	DC	458876.9	4439740.0	6,707	17.2	8.01	0.0	Na–HCO_3
M-57B	132.09	144.03	MC	458875.4	4439742.4	2,360	12.8	8.81	0.0	Na–HCO_3
A-58A1	289	301	AA	461568.2	4443300.1	16,211	18.1	12.67	ND	Na–Cl
A-58A2	208	220	AA	461568.2	4443300.1	15,927	18.2	12.73	ND	Na–Cl
D-60A	280	292	DC	457814.6	4440764.3	525	13.0	8.77	ND	Na–HCO_3
M-60B	114	126	MC	457814.6	4440764.3	573	12.7	9.34	0.0	Na–HCO_3
D-63A	199	211	DC	459207.3	4443039.4	606	18.1	7.91	0.0	Na–HCO_3
D-63B	110.5	122.5	DC	459207.3	4443039.4	641	14.0	8.87	0.0	Na–HCO_3
M-65B	101	117	MC	458254.2	4441658.1	4,175	13.9	12.24	ND	Na–HCO_3
D-68R	63	83	DC	458768.0	4442660.0	739	15.7	8.53	0.0	Na–HCO_3
I-74A	520	544	IA	459431.0	4441041.0	6,919	10.7	8.06	ND	Na–HCO_3
D-74B	282	294	DC	459431.0	4441041.0	23,902	7.8	8.41	ND	Na–Cl
M-74C	78	96	MC	459431.0	4441041.0	6,455	12.4	12.29	ND	Na–HCO_3

Aquifer: *SU* shallow unconfined, *SNU* shallow Neogene unconfined, *MC* middle confined, *DC* deep confined, *AA* Akpinar Aquitard, *IA* Incirlik Aquitard

Chemical characters were taken from SRK (2004). *ND* not determined

 DOI 10.1007/s10040-014-1188-z

concentration and isotopic composition. The samples for CFC analysis were collected following the procedure described by the United States Geological Survey CFC laboratory for the CFC glass bottle method by using 125-ml Boston round clear glass bottles with aluminum-lined plastic caps (US Geological Survey 2011). All samples were collected in duplicate and filled in a 3-l glass beaker so that bottles could be capped under water. The samples were continuously checked for air bubbles; once bubbles were not present, the caps were closed and secured with electrical tape. The bottles were stored upside down until analysis. The noble gas samples were collected by filling 50-cm-long, 1-cm outer diameter copper tubes containing approximately 18 cc of water (Weiss 1968). These tubes were fixed in aluminum channels and sealed at both ends by stainless steel pinch-off clamps. In order to reduce formation of gas bubbles, a back-pressure valve assembly was attached to the discharge end of the copper tubes during sample collection (Stute et al. 1995).

Laboratory analyses

The water samples were analyzed for their $\delta^{18}O$ and δD stable isotope ratios in the Environmental Isotope Laboratory of the University of Waterloo, Canada, by using a Micromass ISOPRIME Continuous Flow Isotope Ratio Mass spectrometer (CF-IRMS). Oxygen-18 determinations were done by CO_2 equilibration using standard procedures (Epstein and Mayeda 1953). The δD measurements were carried out on hydrogen gas produced from water reduced on hot chromium following the procedure described in detail by Drimmie et al. (2001). Analytical uncertainties of the individual measurements are estimated to be within ±0.2 ‰ for $\delta^{18}O$ and ±0.8 ‰ for δD.

Tritium concentrations were determined by the ^{3}He-ingrowth method (Clarke et al. 1976). The tritium samples were degassed and flame-sealed in glass bulbs and stored for more than 4 months. The ^{3}He accumulated from tritium decay was then extracted and measured by using a VG-5400 He isotope mass spectrometer at L-DEO (Ludin et al. 1998). The analytical precision of the tritium measurements was about ±0.1 TU.

CFC-11 and CFC-12 concentrations in water were determined by using a purge and trap system interfaced to a Hewlett- Packard (HP) 5890 series GC (gas chromatograph) system (Smethie et al. 2000). The detection limit was 0.002 pmol per liter of water (pmol/l). Prior to GC analysis the full sample bottles were weighed. The dimensions of the bubbles formed inside the bottles were measured to calculate the volume of gas in the headspace. After the sample was measured on the GC, the dry bottle was weighed again to determine the volume of the water in the original sample. The headspace correction was then applied to calculate the corrected concentrations of measured CFCs, which assumes that the CFCs in the headspace are in thermodynamic equilibrium with the water. The ratio of CFCs in the headspace to CFCs in the water was calculated using the solubility equations determined in Warner and Weiss (1985) and this ratio was applied to the concentration measured in the water.

$^{13}C/^{12}C$ and $^{14}C/^{12}C$ samples were measured from dissolved inorganic carbon (DIC) and analyzed at the National Ocean Sciences Accelerator Mass Spectrometry Facility (NOSAMS; Woods Hole Oceanographic Institution 2011). $^{13}C/^{12}C$ analyses were carried out by using a VG PRISM Stable Isotope Mass Spectrometer. The precision of the measurements are reported to be ±0.05 ‰. $^{14}C/^{12}C$ analyses were carried out by using an accelerator mass spectrometry (AMS) system following the procedures described in Woods Hole Oceanographic Institution (2011) with an analytical precision of ±1 %. The results are reported as percent modern carbon (pmc).

He and Ne were analyzed by using a multi-purpose noble gas mass spectrometer (MAP 215–50) at L-DEO according to the procedures described by Stute et al. (1995). The precision of the measurements is about ±1 to 2 % for noble gas abundances.

Results and discussion

Field chemical data

For the shallow aquifer samples, the electrical conductivity (EC) values varied between 434 μS/cm (S-21) and 14,069 μS/cm (S-9) increasing along flow direction from upgradient to downgradient. For the middle and deep aquifer samples, EC values vary between 573 and 6,455 μS/cm and between 525 and 23,902 μS/cm, respectively, increasing in the direction of the flow due to the presence of a saline zone in the deep system. In this zone, minerals such as searlesite, northupite and shortite are dissolved causing an increase in the concentrations of sodium, chloride and bicarbonate in groundwater (SRK 2004). The abrupt increase in EC values in downstream direction in shallow wells S-4 and S-9 was explained by the upward seepage of deeper groundwater into alluvium in the areas where S-4 and S-9 are located.

pH ranged from 7.53 (S-3) to 8.32 (S-9) in the shallow system, from 8.81 (M-57B) to 12.29 (M-74C) in the middle system, and from 7.57 (D-20) to 9.61 (D-8) in the deep system. Dissolved oxygen contents were between 0.1 mg/l (S-9) and 10 mg/l (S-5) in the shallow system, and <0.05 mg/l in the deeper systems.

$\delta^{18}O$ and δ^2D

Values for stable isotopes of water within the entire aquifer system ranged from −8.10 to −12.80 ‰ and from −60.9 to −92.6 ‰ (V-SMOW) for $\delta^{18}O$ and δD, respectively (Table 2). The isotopically lighter values were observed in the deep aquifer. A strong isotopic contrast is found between shallow and deep aquifer systems, even between the unconfined and the confined parts of the deep aquifer system (Fig. 6; Arslan et al. 2013).

Most of the $\delta^{18}O$ and δ^2H samples from the deeper aquifer systems fall along the Global Meteoric Water Line (GMWL) defined by Craig (1961). However, the values

 DOI 10.1007/s10040-014-1188-z

DOI 10.1007/s10040-014-1188-z

Table 2 Isotopic composition of groundwater from the Kazan Trona Aquifers.

Sample	Aquifer	$\delta^{18}O$ V-SMOW [‰]	$\delta\ ^{2}H$ V-SMOW [‰]	d[a] [‰]	^{3}H [TU]	CFC Conc. [pmol/l]		DIC [mmol/l]	$\delta^{13}C$ V-PDB [‰]	$a^{14}C$ [pmc]	Alk [mg/l] (Camur et al. 2008)	TDS [mg/l] (SRK 2004)
						CFC-11	CFC-12					
S-1	SU	−9.16	−65.69	7.59	5.22	3.403	2.088	ND	ND	ND	318	354.0
S-2	SU	−9.39	−69.21	5.91	2.47	1.069	0.694	ND	ND	ND	366	755.0
S-3	SU	−9.56	−68.61	7.87	6.05	3.165	1.484	ND	ND	ND	431	635.3
S-4	SU	−8.1	−64.57	0.23	0.13	0.408	0.442	9.07	−8.65	29.79	499	1,4100.0
S-5	SU	−9.67	−68.55	8.81	6.96	2.832	1.77	ND	ND	ND	392	537.0
S-9	SU	−10.04	−73.88	6.44	0.02	0.31	0.318	16.39	−8.17	24.00	747	1,950.0
S-11	SU	−9.86	−69.13	9.75	ND	0.789	0.804	ND	ND	ND	388	636.0
S-13	SU	−9.66	−68.82	8.46	5.86	2.34	1.765	ND	ND	ND	458	536.8
S-15	SU	−9.77	−69.39	8.77	ND	1.921	1.584	ND	ND	ND	ND	ND
S-16	SU	−9.88	−69.42	9.62	6.58	2.886	1.927	ND	ND	ND	416	546.0
S-19	SNU	−8.1	−60.89	3.91	14.22	2.673	1.74	ND	ND	ND	464	498.0
S-20	SNU	−9.3	−67.91	6.49	4.96	3.048	2.023	ND	ND	ND	374	430.0
S-21	SNU	−9.08	−67.51	5.13	ND	ND	ND	ND	ND	ND	362	433.0
S-22A	SNU	−8.86	−65.51	5.37	4.44	2.467	1.843	ND	ND	ND	463	532.0
S-23	SNU	−9.37	−68.36	6.6	5.21	2.98	2.005	ND	ND	ND	ND	ND
S-24	SNU	−9.47	−69.2	6.56	ND	2.186	1.532	ND	ND	ND	ND	ND
D-8	DC	−12.31	−88.60	9.88	0.05	ND	ND	12.79	2.28	0.17	2163	2,632.0
D-13	DC	−12.30	−90.07	8.33	0.11	0.065	0.175	12.51	−2.30	0.45	674	864.3
D-20	DC	−10.60	−74.70	10.10	0.32	ND	ND	8.06	−7.01	27.81	409	522.6
D-33	DC	−12.90	−90.80	12.40	ND	0.317	0.456	ND	ND	ND	2,702	3,372.2
D-37	DC	−12.37	−89.60	9.36	0.07	ND	ND	12.01	−3.00	0.29	622	795.0
D-47	DC	−12.50	−92.12	7.88	ND	ND	ND	69.50	2.76	0.15	ND	6,975.0
I-50	IA	−8.99	−74.50	−2.58	0.17	ND	ND	ND	ND	ND	ND	60,633.3
D-53	DC	−8.59	−68.20	0.52	ND	ND	ND	ND	ND	ND	5,639	7,866.3
D-57A	DC	−12.80	−90.30	12.10	0.00	0.049	0.103	95.72	3.52	0.08	5,406	7,505.6
M-57B	MC	−12.70	−92.60	9.00	ND	ND	ND	ND	ND	ND	2,542	3,518.9
A-58A1	AA	−11.40	−82.40	8.80	ND	ND	ND	ND	ND	ND	ND	6,706.0
A-58A2	AA	−11.60	−82.80	10.00	ND	ND	ND	ND	ND	ND	ND	6,372.0
D-60A	DC	−12.50	−90.99	9.01	0.07	ND	ND	ND	ND	ND	398	495.8
M-60B	MC	−12.54	−90.60	9.72	0.09	0.073	0.176	7.07	−6.64	0.39	485	606.0
D-63A	DC	−11.00	−78.70	9.30	0.05	0.487	0.559	7.80	−7.74	3.70	386	421.8
D-63B	DC	−11.40	−82.23	8.97	ND	0.373	0.241	ND	ND	ND	453	637.8
M-65B	MC	−9.72	−72.90	4.86	ND	ND	ND	ND	ND	ND	2,324	2,835.0
D-68R	DC	−12.25	−89.00	9.00	0.04	0.483	0.231	7.71	−6.33	0.80	391	699.0
I-74A	IA	−11.90	−90.10	5.10	ND	ND	ND	ND	ND	ND	ND	7,273.3
D-74B	DC	−8.65	−67.80	1.40	ND	ND	ND	ND	ND	ND	991	14,773.0
M-74C	MC	−10.00	−76.90	3.10	ND	ND	ND	ND	ND	ND	2,408	3,356.7

Aquifer: *SU* shallow unconfined, *SNU* shallow Neogene unconfined, *MC* middle confined, *DC* deep confined

[a] d is the deuterium excess value and is defined as $d=\delta D-8\delta^{18}O$

from the shallow wells show deviations from the GMWL (Arslan et al. 2013). The deviations from the GMWL are probably caused by evaporative enrichment of these samples since the depth to groundwater is between 2 and 15 m in those wells (less than 2 m in well S-9 and around 15 m in S-5). Such evaporative enrichment frequently occurs during or after recharge in arid regions (e.g. Clark and Fritz 1997).

Origin and apparent ages of groundwater

Monthly weighted mean values (MWMAP) of stable isotopic composition in rainfall were obtained from the nearest isotope monitoring station operated by International Atomic Agency/ World Meteorological Organization (Global Network of Isotopes in Precipitation 2006) located in Ankara at an altitude of 902 m between 1963 and 2006 (Fig. 6). Precipitation during March and November is more enriched in stable isotopic compositions compared to precipitation in December, January and February. Although MWMAP values of precipitation for other months are not included in Fig. 6, they are more enriched than precipitation in March and November (up to −4 ‰ and −25 ‰ for $\delta^{18}O$ and δD, respectively). The monthly distribution of precipitation data shows that two-thirds of the annual precipitation occurs during the winter and spring seasons (December and May), whereas the rest occurs in the summer and fall seasons. The isotopic signature of modern groundwater from the shallow aquifer system is consistent with local precipitation received in March and November despite the evaporative enrichment effects. On the other hand, the stable isotopic composition of the deeper groundwater is more depleted than the shallow groundwater samples and MWMAP values of winter precipitation (Fig. 6). Part of this depletion is due to the fact that there is a recharge elevation difference between modern recharge samples and deep aquifer samples. However, it is not possible to explain the average isotopic depletion of 2.5 ‰ measured in samples from most of the deeper groundwater systems only with the altitude effect if the relationship between $\delta^{18}O$ and elevation obtained by Apaydin (2004) for Beypazari Trona Ore field, located 50 km west of the study area is used (Arslan et al. 2013). According to Apaydin (2004), the depletion in $\delta^{18}O$ is about 0.44 ‰ per 100 m rise in altitude. This finding, together with the deviations of the samples from the GMWL, raises the question whether these waters represent present-day recharge or if they were recharged during a different climatic period than today's with colder temperatures and/or with higher precipitation amounts. This issue is discussed in detail in Arslan et al. (2013) who conclude that the lighter stable isotope values in deeper aquifers reflect both altitude and temperature effects. Arslan et al. (2013) estimated that the approximate elevation difference between shallow and deep groundwater systems is 200 m; therefore, about 0.9 ‰ of the depletion would be due to the elevation effect and 1.6 ‰ is a lower limit for the climate-induced change.

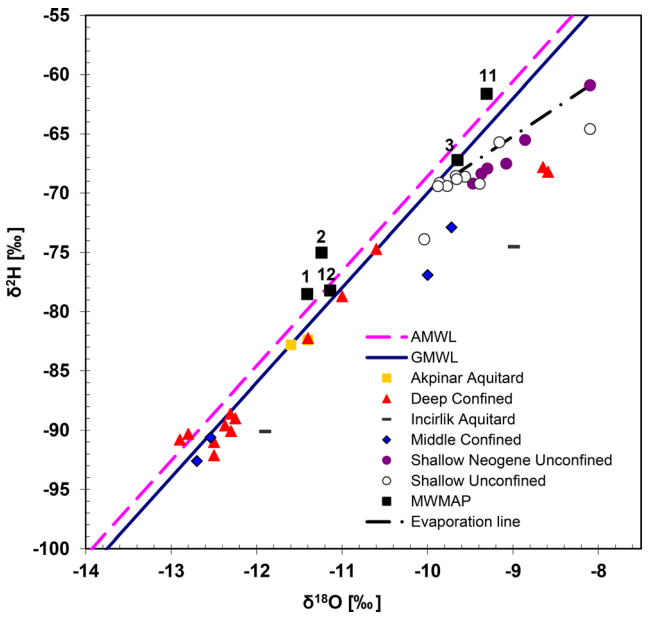

Fig. 6 δ^2H vs. $\delta^{18}O$ diagram. *GMWL* Global Meteoric Water Line (Craig 1961); *AMWL* Ankara Meteoric Water Line equation calculated from data in IAEA/WMO, 2004 ($\delta^2H=8\delta^{18}O+11.42$); MWMAP (monthly weighted mean of Ankara Precipitation (IAEA/WMO, 2004); the numbers *1*, *2*, *3*, *11* and *12* refer to calendar months January, February, March, November and December, respectively] (Arslan et al. 2013)

CFC and $^3H/^3He$ ages

Samples from the shallow aquifer display CFC concentrations that range from 0.31 to 3.40 pmol/l and tritium concentrations from 0.14 TU to 13.45 TU. Concentrations of these tracers are near their detection limits for the deep aquifer system (Fig. 7).Apparent CFC ages of groundwater in the Kazan aquifer system, i.e., the time elapsed since isolation of newly recharged water from the soil air (Plummer and Busenberg 2000), were estimated using measured concentrations of CFC-11 (trichlorofluoromethane: $CFCl_3$) and CFC-12 (dichlorodifluoromethane: CF_2Cl_2). The apparent CFC ages were calculated by dividing the measured CFC concentrations by the solubility at the recharge temperature, yielding the atmospheric concentration at the time of recharge, assuming the recharged water was in equilibrium with the atmosphere and no local CFC excess above remote atmosphere concentrations was present. This concentration was compared to the atmospheric time history given by Bullister (2011) to obtain the time of recharge. The estimates of recharge temperatures and excess air for samples S-2, S-3, S-4, S-5, S-9, S-11, S-16, S-19, D-8, D-13, D-33, D-37, D-47, and D-68R were obtained from noble gas measurements using the closed system equilibration (CE) model (Aeschbach-Hertig et al. 2000). The calculations are explained in detail in Arslan et al. (2013). For the remaining shallow aquifer samples, the water recharge temperature was assumed to be 13 °C,

DOI 10.1007/s10040-014-1188-z

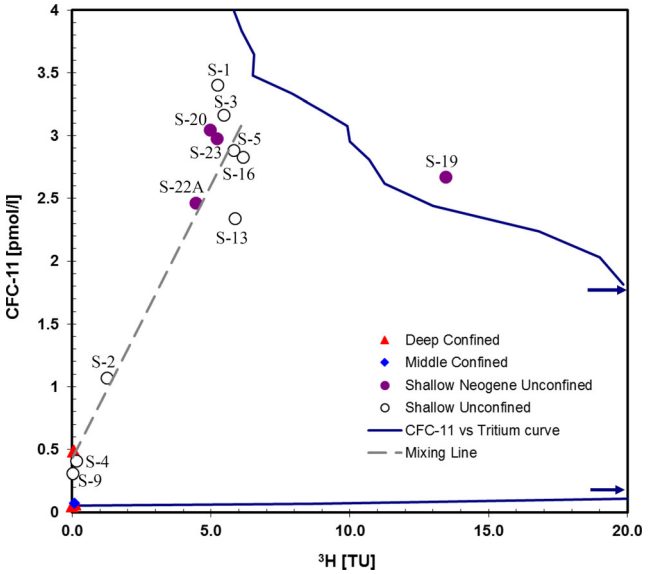

Fig. 7 CFC-11 vs ^{3}H concentrations. The CFC-11 vs tritium curve is prepared by using the CFC concentrations representing the water entering the system at a particular time without being affected by any processes such as sorption, mixing etc. The tritium concentrations used for the temporal evolution of tritium in precipitation are obtained from the IAEA/WMO Ankara station tritium data and correcting them for radioactive decay. The *broken line* represents the mixing of younger shallow groundwater and older deep groundwater. See text for discussion

which is the current average yearly ground temperature calculated by using the daily soil temperature measurements at Ankara station (elevation: 891 m) and correcting them for the decrease in temperature from 891 to 1,050 m. These measurements were taken 50 cm below ground between 1941 and 2006 (The Turkish State Meteorological Service, personal communication, 2012). For the remaining deep aquifer samples (D-57A, M-60B, D-63B), a recharge temperature of 8 °C was assumed because deep aquifer samples have lower recharge temperatures when compared to the shallow aquifer samples based on noble gas data. A change in the recharge temperature does not affect the CFC ages from the deep aquifer system because CFC concentrations in these three samples are close to the detection limit. Additionally, CFC ages cannot be calculated for D-57A and D-63B even if the recharge temperatures are modified due to the low dissolved concentrations of CFCs.

Excess-air concentrations vary between 1.9 and 108.3 ccSTP/kg in the shallow aquifer system (Table 3). This large range makes it difficult to estimate the amount of excess air for the samples where noble gas data are not available. Air entrapment effects the CFC recharge years, especially in shallow wells. For instance, for S-1, CFC-11 and CFC-12 recharge years are 1985.5 and 1992, respectively when the calculations are carried out by assuming no excess air is present (the difference is 6.5 years). If 40 cc/kg of excess air is assumed to be present in the sample, then CFC-11 and CFC-12 ages become equal, both of them being 1983. For S-24, this difference amounts to 7.5 years when excess air is neglected (CFC-11 and CFC-12 recharge years would be 1977 and 1984.5, respectively); however, under the presence of 60 cc/kg excess air, the difference is 0.5 years, years, recharge years for CFC-11 and CFC-12 being 1975 and 1975.5, respectively. A change in excess air effects CFC-12 ages more, because CFC-12 is less soluble than CFC-11. Herein, for those shallow water samples where no noble gas data is available, the calculations were made by using the average excess air (18 cc/kg).

The recharge elevations used in the calculations are 1,050 m for shallow aquifer samples and 1,250 m for samples from the deeper systems. The calculated recharge years range from 1963 to 1987 for the shallow aquifer system. CFC-12 ages are 2—7 years lower than CFC-11 ages in the shallow aquifer system, except for groundwaters in S-2 and S-3, where the CFC 11 and CFC 12 ages are equal to each other, and S-1, S-16 and S-24 where the CFC-11 ages are lower than the CFC-12 age (Table 3). The inconsistency between these ages indicates involvement of different processes such as loss of CFC-11 during microbial degradation in anaerobic environments (e.g., Shapiro et al. 1997; Plummer and Busenberg 2000) or enrichment of CFC-12 due to dissolution of air trapped during recharge since CFC-12 has a lower solubility than CFC-11 (Cook et al. 2003). Degradation of CFC-11 is unlikely in the shallow aquifer system since groundwater contains dissolved oxygen (Table 1). Further investigations are needed to support air entrapment effects on CFC concentrations in the shallow aquifer samples that have no noble gas data.

There is a positive correlation between the measured CFC-11 and tritium concentrations of the groundwater samples in the area (Fig. 7). In Fig. 7, CFC-11 vs tritium curve is also plotted in which the atmospheric CFC-11 source functions measured in the northern hemisphere were converted into dissolved concentrations using Henry's law and the tritium concentrations are calculated on a yearly basis by using the tritium values measured in precipitation at the Ankara IAEA/WMO station. These values are smoothed by calculating the 5-year running average for each year after reducing the ^{3}H concentrations to take into account the radioactive decay until sampling occurred in 2006. Some data points plot on this curve indicating minimal mixing (e.g. S-19, S-3, S-16). However, many other samples do show mixing between young (22 years) and older groundwater (without tritium or CFC-11) (e.g., samples S-2 and S-13). Two samples (S-4 and S-9) having the highest TDS values and lowest DO contents among shallow wells (Table 1) mark the starting point for the mixing line and they represent a huge contribution from older groundwater. This finding is also supported by Camur et al. (2008) who explained chemical anomalies (e.g. abrupt changes in electrical conductivity of up to 14,000 mg/l and elevated concentrations of B up to 22 mg/l, Cl up to 3,000 mg/l and SO_4 up to 6,200 mg/l) in S-4 and S-9 groundwater compositions as the result of mixing of shallow and deeper groundwater. Herein, it should be emphasized that the broken line in Fig. 7 ideally starts from a sampling point where there is no tritium and

DOI 10.1007/s10040-014-1188-z

Hydrogeology Journal (2015) 23: 175–194

DOI 10.1007/s10040-014-1188-z

Table 3 The recharge temperatures and elevations used in the calculations (details of which can be found in Arslan et al. 2013), the CFC-11 and CFC-12 recharge years and the corrected ^{14}C ages together with the activities of initial ^{14}C assigned to each sample and the dilution factors (*ND* not determined)

Sample	Aquifer	Rech. Temp. [°C]	Rech. Elev. [m]	Excess air [cc/kg]	^{3}H [TU]	CFC recharge year		Mean CFC age [years]	$\delta^{13}C$ [‰]	$a_0{}^{14}C_{DIC}$ [pmc]	Dilution factor	Corrected ^{14}C Age[a] [years]	$^{3}H/^{3}He$ age [years]	Binary fraction of young water from tritium	Binary fraction of young water from CFC-11
						CFC-11	CFC-12								
S-1	SU	13	1,050	18.2	5.22	1984.5	1987	21	ND	ND	ND	ND	ND	ND	ND
S-2	SU	11.6	1,050	23.3	1.25	1970	1970	37	ND	ND	ND	ND	23.9	0.28	0.33
S-3	SU	11.8	1,050	1.9	5.45	1982.5	1982.5	25	ND	ND	ND	ND	ND	ND	ND
S-4	SU	14.3	1,050	2.1	0.14	1965.5	1969	40	−8.65	68	0.41	−600	ND	ND	ND
S-5	SU	14.7	1,050	10.8	6.16	1983	1987	22	ND	ND	ND	ND	0.8	0.72	0.79
S-9	SU	10.2	1,050	5.1	0.02	1962.5	1965	44	−8.17	68	0.39	900	ND	ND	ND
S-11	SU	12.4	1,050	8	ND	1968.5	1973	36	ND	ND	ND	ND	ND	ND	ND
S-13	SU	13	1,050	18.2	5.86	1977	1984	27	ND	ND	ND	ND	ND	ND	ND
S-15	SU	13	1,050	18.2	ND	1975	1981.5	29	ND	ND	ND	ND	ND	ND	ND
S-16	SU	13.9	1,050	108.3	5.81	1977.5	1975	31	ND	ND	ND	ND	2.2	0.73	0.58
S-19	SNU	13.4	1,050	2.4	13.45	1981	1987	23	ND	ND	ND	ND	8.5	2.09	0.66
S-20	SNU	13	1,050	18.2	4.96	1982	1986.5	23	ND	ND	ND	ND	ND	ND	ND
S-22A	SNU	13	1,050	18.2	4.44	1978	1985.5	26	ND	ND	ND	ND	ND	ND	ND
S-23	SNU	13	1,050	18.2	5.21	1982	1985.5	24	ND	ND	ND	ND	ND	ND	ND
S-24	SNU	13	1,050	18.2	ND	1976	1981	29	ND	ND	ND	ND	ND	ND	ND
D-8	DC	6.2	1,250	ND	0.05	ND	ND	ND	2.28	68	0.06	2500	ND	ND	ND
D-13	DC	5.4	1,250	9.8	0.11	ND	ND	ND	−2.3	68	0.2	28300	ND	ND	ND
D-20	DC	ND	1,250	ND	0.32	ND	ND	ND	−7.01	68	0.36	−1100	ND	ND	ND
D-33	DC	8.5	1,250	22	ND	1961	1965.5	44	ND	ND	ND	ND	ND	ND	ND
D-37	DC	5.2	1,250	ND	0.07	ND	ND	ND	−3	68	0.23	32800	ND	ND	ND
D-47	DC	8.5	1,250	ND	ND	ND	ND	ND	2.76	68	0.04	23800	ND	ND	ND
D-57A	DC	8	1,250	ND	0	ND	ND	ND	3.52	68	0.02	21900	ND	ND	ND
M-60B	MC	8	1,250	18.2	0.09	1955	1959	50	−6.64	68	0.34	33900	ND	ND	ND
D-63A	DC	4.1	1,250	ND	0.05	ND	ND	ND	−7.74	68	0.38	16000	ND	ND	ND
D-63B	DC	8	1,250	ND	ND	ND	ND	ND	ND	ND	ND	ND	ND	ND	ND
D-68R	DC	3.2	1,250	6.6	0.04	1964.5	1962	44	−6.33	68	0.33	27700	ND	ND	ND

[a] ^{14}C age calculated according to Pearson and Hanshaw (1970) assuming $\delta^{13}C$ values of −27 ‰ and +4 ‰ for soil CO_2 and carbonates, respectively and ^{14}C activity of 0 pmc for carbonates

CFC-11 present. However, there is some CFC-11 present in samples S-4 and S-9, although these samples are tritium-free. The presence of CFC-11 might be due to a slight contamination of these samples during sampling because sampling was carried out by using a plastic hose. Plastic materials used in casing of the wells or during sampling might cause contamination of the water samples with CFC's (Dunkle et al. 1993; Plummer et al. 2006).

Like the CFC's, ^{3}H and ^{3}He are useful to date young groundwaters as demonstrated by Schlosser et al. (1988, 1989), Poreda et al. (1988), Aeschbach-Hertig et al. (1998), among others. In this study, due to the complex mixing mechanisms between the deeper, older groundwater and recently recharged, younger (shallow) groundwater; a high terrigenous helium component is present in most of the samples (Fig. 8). Therefore, it is feasible to calculate $^{3}H/^{3}He$ ages only for four samples from the shallow system ranging from 0.8 to 23.9 years. The $^{3}H/^{3}He$ ages calculated for samples S-16, S-19 and S-5 are very different from the corresponding CFC ages (Table 3). To check whether the $^{3}H/^{3}He$ ages from the samples have been significantly influenced by mixing, the reconstructed original tritium concentrations of the water samples were compared with historical records of the tritium concentration as explained by Dunkle et al. (1993) and Stute et al. (1997). For this purpose, the tritium records from the IAEA network Ankara station and the data points from the four aforementioned wells are superimposed on the input history by using the time of infiltration calculated as sampling date minus $^{3}H/^{3}He$ age vs the measured tritium concentration and the ^{3}H at the time of infiltration ($^{3}H + {}^{3}He_{trit}$; Fig. 9). In this figure, if the water is not influenced by mixing or loss of ^{3}He, all initial tritium points should fall on the input curve. From Fig. 9 it is clear that for S-2 there is mixing of older groundwater because the initial tritium value of this sample falls below the input curve. The $^{3}H/^{3}He$ age of a mixture of pre-bomb water free of both tritium and tritiogenic ^{3}He and a water parcel containing tritium and tritiogenic ^{3}He would be the same as that of the young component because dilution would not alter the ratio of tritium and tritiogenic ^{3}He (Jenkins and Clarke 1976). Therefore, the $^{3}H/^{3}He$ age of this sample represents the age of the young component, assuming a two-component mixture. The other samples that fall slightly below the tritium input curve are S-16 and S-5. There is deviation of the initial tritium concentration observed in S-19, a well with the highest tritium concentrations (Fig. 9). S-19, unlike S-2, S-5 and S-16, is a well penetrating a Neogene perched aquifer and the Neogene units are not as permeable as the alluvium in the study area (SRK 2004). Therefore, for sample S-19, water from a range of infiltration times might be present causing this deviation in Fig. 9.

The mixing fractions of young and old water can be approximated with a binary-dilution model using the $^{3}H/^{3}He$ ages of young component in the sample (Yager et al. 2013). The ratio of initial tritium in the sample and the amount of tritium in precipitation at the time of recharge, where the recharge date is the $^{3}H/^{3}He$ age, would give the fraction of young water. The tritium amount in the precipitation varies seasonally, and it is not possible to estimate the value better than ±10 % (Yager et al. 2013) although initial tritium can be measured quite accurately. The fraction of young water can also be

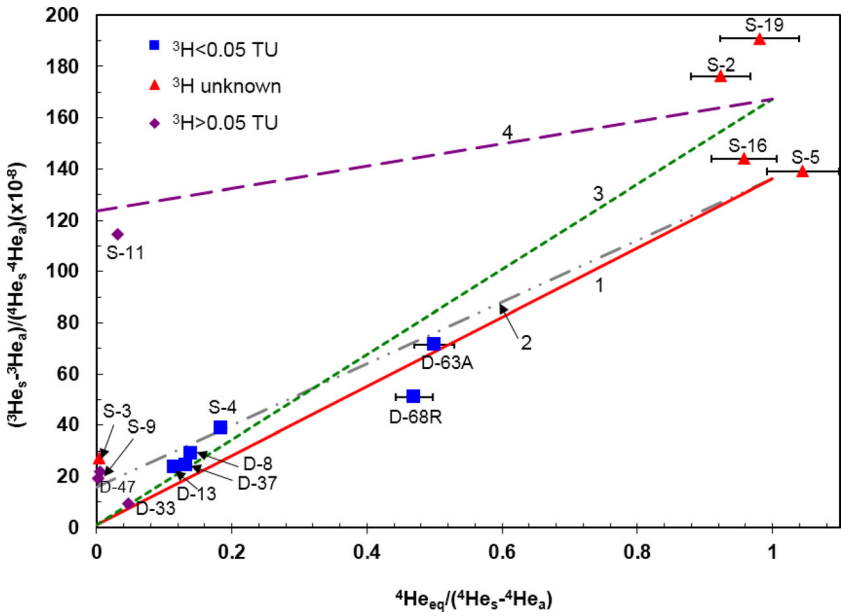

Fig. 8 Measured $^{3}H/^{4}He$ ratio corrected for excess air as a function of the relative amount of helium due to solubility equilibrium with respect to total helium corrected for excess air. Line *1* represents the evolution of the ratios with $^{3}He/^{4}He$ crustal ratio of 2×10^{-8}. An additional 1 % mantle helium shifts line *1* to line *2*. No He of tritiogenic origin is present in these cases. Line *3* shows the evolution of line *1* when 5 TU is added and totally decayed to produce 1.25×10^{-14} cm^{3} STP/gTU of $^{3}He_{trit}$ together with an average crustal production $^{3}He/^{4}He$ ratio of 2×10^{-8}. Line *3* shifts to line *4* with an addition of 10 % mantle helium ($^{3}He/^{4}He=1.2\times10^{-5}$). Data points above lines *1*, *2* and *3* identify samples that contain either mantle-derived helium or $^{3}He_{trit}$ produced by decay of bomb tritium

 DOI 10.1007/s10040-014-1188-z

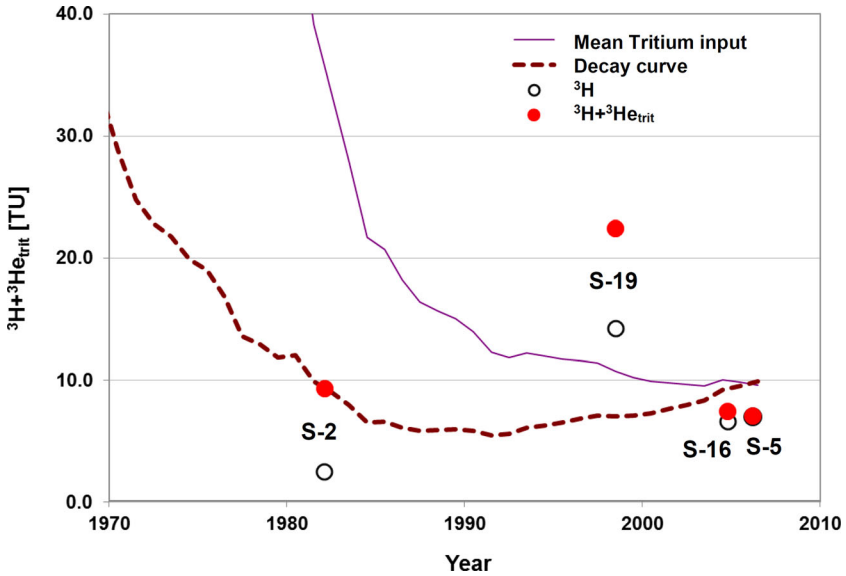

Fig. 9 Comparison of the measured tritium and "initial tritium" (^{3}H + ^{3}He$_{trit}$) concentrations of the samples and the moving average of the tritium input history recorded at the Ankara IAEA station. All data points are discussed in the text

calculated sensitively by using CFC-11 concentrations. The ratio of the CFC-11 concentration in the sample to the atmospheric concentration of CFC-11 at the time of recharge (based on the apparent ^{3}H/^{3}He age) would give the young water fraction (Yager et al. 2013). The binary fractions of young water from tritium and CFC-11 are calculated for four of the samples for which ^{3}H/^{3}He ages are available (S-2, S-5, S-16 and S-19). They vary between 0.33 and 0.79 for the ones calculated by using CFC-11 data and vary between 0.28–2.09 for the ones calculated by using tritium data. These fractions are in agreement with each other (Fig. 10) except for S-19. In S-19, according to the tritium data, the fraction of young water is more than 200 %, which is not a reasonable estimate. Therefore, it can be concluded that for S-19 there is tritium contamination most likely during sampling.

The CFC ages are higher for the deep and middle aquifer systems if compared to the shallow system. Although it is possible to assign apparent ages to the samples of the middle and deep groundwater systems, these ages can be deceptive because the CFC concentrations measured in those samples are very close to the detection limit. It was also impossible to assign ^{3}H/^{3}He ages to the samples from the deep aquifer system because they have low ^{3}H concentrations and contain large excesses of terrigenic helium. Thus, these waters were dated with the radiocarbon method (measurement of ^{13}C and ^{14}C in DIC) which allows for the dating of groundwater with ages up to 40,000 years BP.

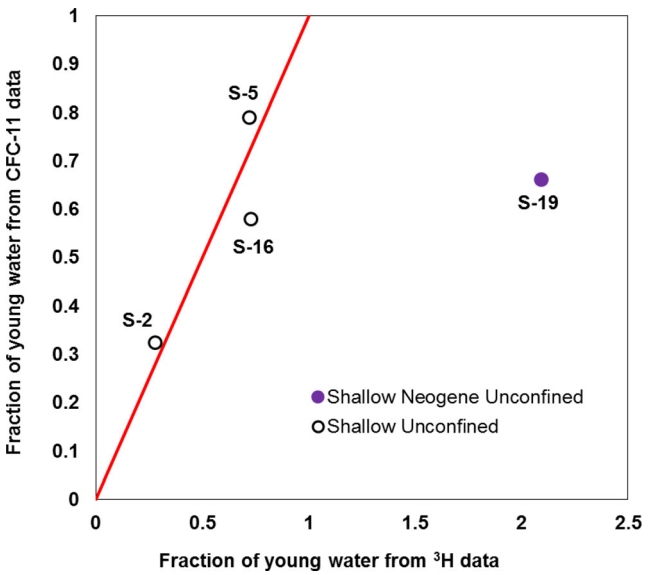

Fig. 10 Comparison of fractions of young water based on ^{3}H and on CFC-11. See text for details

^{14}C ages

Radiocarbon dating of groundwater is based on measuring the loss of the parent radionuclide ^{14}C and depends on knowing the initial activity of the DIC resulting from a mixture of soil CO_2 with variable ^{14}C and solid carbonate having ^{14}C values close to zero. The ^{14}C activities of a total of 11 samples collected from the shallow and deep wells range from 29.79 to 0.08 pmc, the ones close to the detection limit (0.07 pmc) belonging to the deep system. The ^{14}C age calculations for the Kazan Trona aquifer system had been discussed in detail in Arslan et al. (2013); therefore, a brief summary will be given herein. There is enrichment in δ^{13}C values and depletion in δ^{18}O values with decreasing ^{14}C activities (e.g. Fig. 11). Due to intensive water–rock interaction as indicated by δ^{13}C data ranging from −8.65 to +3.52 ‰ (more enriched values are observed in the deep aquifer) and addition of dead carbon to most of the samples, a δ^{13}C mixing model was used (Pearson 1965; Pearson and Hanshaw 1970) to correct the ^{14}C ages. The initial ^{14}C activity ($a_0{}^{14}$C) given in Table 3 as 68 pmc is estimated by

DOI 10.1007/s10040-014-1188-z

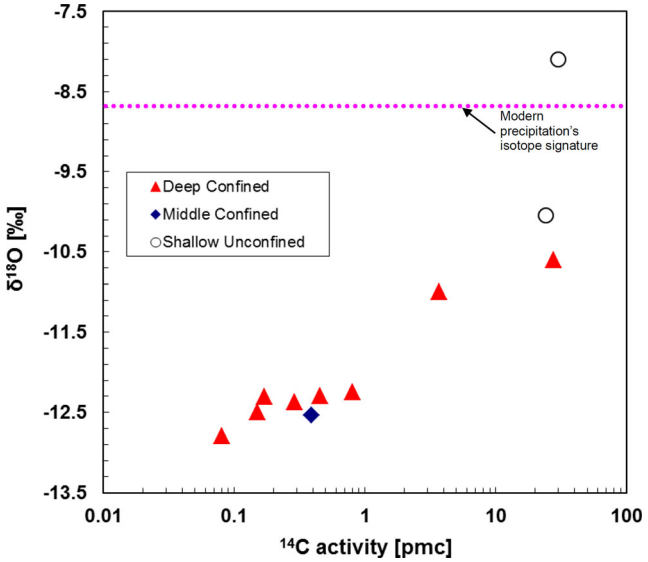

Fig. 11 $\delta^{18}O$ (‰) vs ^{14}C activity (pmc). The oxygen-18 content of modern precipitation is also shown ($\delta^{18}O$=−8.65 ‰)

using radiocarbon data of a seasonal spring that is proven to be modern by Yazicigil et al. (2001). This spring responds to precipitation immediately and ceases to flow during the dry season. For this spring (SP-2 in Fig. 2), the ^{3}H amount, ^{14}C activity, and the $\delta^{13}C$ value were reported to be 7.58 TU, 68 pmc and −8.96 ‰, respectively in February 2001. While assigning the a_0 ^{14}C value, there was awareness of the fact that this sample contains tritium and there would be an overestimation of the initial condition because of the presence of bomb ^{14}C.

A dilution factor (q) was used in the calculations as a measure of carbonate dissolution in the aquifer (Pearson and Hanshaw 1970) (Table 3). When determining the dilution factors, $\delta^{13}C$ of the carbonates ($\delta^{13}C_{carb}$) in the study area is assigned as +4 ‰ by referring to the analysis results obtained by Bayari et al. (2009) for Mesozoic dolomitic limestones in Konya Closed Basin located in Central Anatolia. $\delta^{13}C$ value of soil CO_2 ($\delta^{13}C_{soil}$) was assigned as −27 ‰ since the plant species in the study area follow a C_3 pathway as their principal photosynthesis cycle according to the field studies carried out by Cetin et al. (2002) and this value should have been constant between 30,000 and 15,000 years BP according to pollen evidence from western Turkey (Bottema and van Zeist 1981; Prentice et al. 1992; Wick et al. 2003). According to Table 3, the estimates of ages through ^{14}C dating range from modern to ~34 thousand years (ka) BP and all the samples from the middle and deep aquifer systems, except for sample D-20, entered the system before the Holocene. This observation is consistent with the findings extracted from the noble gas data (Arslan et al. 2013). It should be noted that the age estimates derived from ^{14}C dating in this study are likely lower limits because most measurements are only slightly above the detection limit. Additionally, Arslan et al. (2013) noted that, except for one sample (D-47), samples from the deep aquifer are consistent with the accumulation of internally produced radiogenic ^{4}He released by the decay of U/Th, which increases with groundwater residence time. Indeed, He excess suggests that only for D-47 the mean residence time should be lower than the radiocarbon age presented herein (Arslan et al. 2013).

Helium components in groundwater of the Kazan Trona Basin

Helium isotopes have proven very useful in a wide variety of groundwater studies due to their conservative nature and their known source functions (Marty et al. 1993). Dissolved helium in excess of the equilibrium with the atmosphere found in continental groundwaters is usually generated by radioactivity and other nuclear processes within the crust. This helium is established by its distinct isotopic composition as its $^{3}He/^{4}He$ ratio is approximately $2\times10^{-8}=0.02R_A$ (e.g., Mamyrin and Tolstikhin 1984; R_A is the atmospheric $^{3}He/^{4}He$ ratio of 1.384×10^{-6}, Clarke et al. 1976). In areas where mantle volatiles escape through the crust and accumulate in groundwater, the isotopic composition will be $^{3}He/^{4}He\approx1.2\times10^{-5}=8R_A$ (e.g., Mamyrin and Tolstikhin 1984). The most important sources of helium isotopes in aquifers are the α-decay of U and Th series elements in common rocks (accumulating $^{4}He_{rad}$), β-decay of natural and bomb tritium (^{3}H) (accumulating $^{3}He_{trit}$) and thermal neutron activation of ^{6}Li in the solid phase (producing ^{3}H and then $^{3}He_{nuc}$). Measured sample concentrations (i.e. $^{3}He_{tot}$ and $^{4}He_{tot}$) represent the sum of tritiogenic He ($^{3}He_{trit}$), air-equilibrated He (He_{eq}), He from dissolved air bubbles (He_{exc}), mantle He (He_{mantle}) and crustal He (He_{crust}).

Groundwater samples in this study display a wide range of helium concentrations between 5.04×10^{-8} cm^3 STP/g and 1531×10^{-8} cm^3 STP/g (Table 4). $^{3}He/^{4}He$ ratios changes between $0.09R_A$ and $1.29R_A$. The highest ratios were found in young groundwater from the shallow aquifer, the lowest ones in old groundwater from the deep aquifer.

The $^{3}He/^{4}He$ ratio of helium dissolved in groundwater can be expressed as

$$\left(\frac{^{3}He}{^{4}He}\right)_{tot}=\frac{^{3}He_{eq}+^{3}He_{exc}+^{3}He_{tri}+^{3}He_{crust}+^{3}He_{mantle}}{^{4}He_{eq}+^{4}He_{exc}+^{4}He_{crust}+^{4}He_{mantle}} \quad (1)$$

Weise (1986) introduced a linear equation to illuminate the contribution of the individual He sources to the measured He concentrations and $^{3}He/^{4}He$ ratios (Eq. 2; see also Weise and Moser 1987; Stute et al. 1992b; Castro et al. 2000 and Torgersen and Stute 2013).

$$\left(\frac{^{3}He_{tot}-^{3}He_{eq}}{^{4}He_{tot}-^{4}He_{eq}}\right)=\left[R_{eq}-R_{terr}+\frac{^{3}He_{tri}}{^{4}He_{eq}}\right].\frac{^{3}He_{eq}}{^{4}He_{tot}+^{4}He_{eq}}+R_{terr} \quad (2)$$

DOI 10.1007/s10040-014-1188-z

Table 4 Helium and neon data for the Kazan Trona Basin

Sample	^4He_s (10^{-7}) cm^3 STP/g	Ne_s (10^{-7}) cm^3 STP/g	Ne_a (10^{-7}) cm^3 STP/g	^4He_a (10^{-7}) cm^3 STP/g	$^4He_{ex}$ (10^{-7}) cm^3 STP/g	R_s/R_A
Shallow aquifer						
S-2	0.50	2.01	0.28	0.07	0.03	1.24
S-3	120.43	2.13	0.39	0.60	119	0.2
S-4	2.22	2.03	0.36	0.10	1.73	0.31
S-5	0.46	1.99	0.31	0.08	−0.02	1
S-9	75.45	2.29	0.56	0.10	75	0.16
S-11	13.17	2.41	0.69	0.20	12.6	0.83
S-16	0.51	2.08	0.38	0.09	0.02	1.03
Shallow Neogene aquifer						
S-19	0.54	2.18	0.48	0.13	0.01	1.29
Deep aquifer						
D-8	3.19	3.06	1.28	0.33	2.46	0.29
D-13	3.80	2.85	1.06	0.29	3.11	0.23
D-33	8.64	2.67	0.94	0.24	8.01	0.09
D-37	3.33	2.82	1.02	0.28	2.65	0.25
D-47	153.14	2.84	1.10	0.60	152	0.14
D-63A	11.247	3.02	–	–	–	0.65
D-68R	1.21	3.04	1.20	0.34	0.46	0.55

where, R_{terr} represents the $^3He/^4He$ ratio originating from the terrigenic sources (crust and mantle):

$$R_{terr} = \left(\frac{^3He}{^4He}\right)_{terr} = \frac{^3He_{nuc} + {}^3He_{mantle}}{^4He_{rad} + {}^4He_{mantle}} \quad (3)$$

In Eq. (2), the y-axis is the measured $^3He/^4He$ isotope ratio corrected for the excess air addition and the x-axis is the fraction of ^4He in water resulting from air-equilibration with respect to the total ^4He, corrected for excess air.

In Fig. 8, this method is illustrated by plotting y vs x for Kazan Trona Basin data to estimate R_{terr} value (the y-axis intercept) which represents the contribution of helium originating from crustal and mantle fluxes. The $^4He_{eq}$ and $^4He_{exc}$ values were obtained from the inverse modeling calculations as defined by Aeschbach-Hertig et al. (2000), the details of which can be found in a companion work (Arslan et al. 2013).

In Fig. 8, if data points are present above lines 1, 2, 3 and 4 (like S-2 and S-19) significant amounts of bomb tritium must be present in these samples causing the accumulation of $^3He_{trit}$. The $^3He_{trit}$ component of samples S-2, S-5, S-16 and S-19 were investigated in the preceding section. In this figure, except for samples D-68R, S-2 and S-19, all the samples plot between lines 1 and 4. If R_{crust} is assumed to be constant throughout the study area, data points above line 1 contain either $^3He_{trit}$ or He_{mantle}. Except for S-3, all the samples plotted towards the left side of the x-axis do not contain tritium. For samples characterized by $^3H<0.05$ TU falling above lines 1 and 3 should contain significant amounts of mantle helium. Unfortunately, no information is available about the tritium content of the samples D-47 and S-11. If it is assumed that the shift of S-3, S-9 and S-11 from line 1 is due to the accumulation of $^3He_{trit}$ from the decay of tritium, then the initial tritium contents should approximately be 1,240, 600 and 575 TU, respectively, which are unreasonably high. It is interesting to observe that these three data points lie just around the suspected fault line passing between Incirlik and Dutluca villages (Figs. 2 and 4) that may likely cause deeper groundwater water to move upwards. When the intensely fractured sections of the deep aquifer system are considered, the mechanism transporting these huge amounts of He_{mantle} to the shallower parts should be different line sources. In addition to the fractures, the upward mixing of the deeper groundwater along the NE–SW striking fault enhances the dissemination of different helium components to the shallower parts. The presence of even minor amounts of He_{mantle} indicates the heterogeneity of the whole system and the existence of pathways for He from mantle to even shallower parts in the study area. Under these circumstances, it is logical to claim that these three samples contain different amounts of mantle-derived helium (1–9 % mantle helium). The complex mixing theory is also supported by the CFC and tritium data. For remaining samples (S-4, D-63A, D-8, D-37, D-13 and D-33) the majority of helium present is of crustal origin with some contribution of mantle helium flux.

Conceptual flow model of the groundwater system

The findings presented in the preceding sections confirm the presence of three aquifer systems over the Kazan Trona basin and suggest a mixing mechanism along a suspected buried fault that extends in NE–SW direction (Fig. 4). Borehole data proposed the presence of this buried fault during geological studies carried out by Rojay et al. (2002). No slip data were obtained to justify the existence of the fault geologically. Hence, this study has proved the existence of this fault and the mixing mechanisms along the fault. The existence of this fault along the downgradient flow direction forms an avenue

DOI 10.1007/s10040-014-1188-z

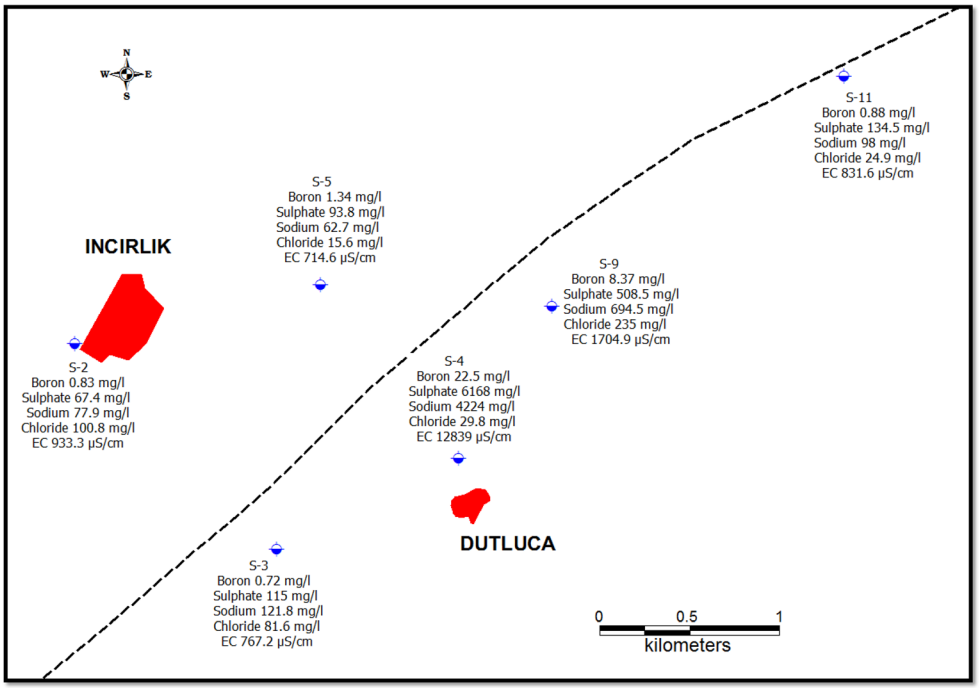

Fig. 12 Map showing concentrations of boron, sulphate, sodium, chloride and electrical conductivity (EC) in selected wells located upstream and downstream from the probable fault. Chemistry data was taken from Arslan (2008)

for the poorer quality deeper groundwater to flow upward and mix with the high quality shallow aquifer system groundwater. The groundwater quality in the shallow system to the southeast of the fault line is strongly affected by this mixing mechanism as proven by the abruptly elevated values of electrical conductivity, boron, chloride and sulphate ions (Fig. 12). These wells are characterized by low tritium contents and CFC concentrations and also by high He-excess values (Fig. 13) due to contribution from deeper, older groundwater along the buried fault. He-excess values increase remarkably because there is mantle-He escape along the fault line. On the other hand, shallow wells located upstream of the suspected fault exhibit low B, SO_4, Na and Cl concentrations together with high amounts of dissolved CFCs and tritium (Fig. 13). He-excesses are very close to 0 and He present

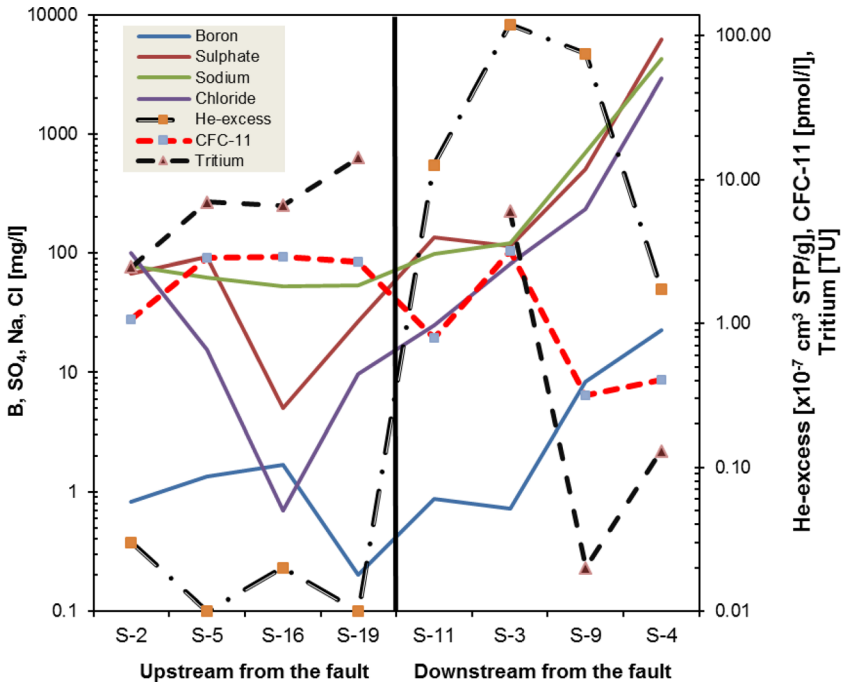

Fig. 13 Boron, sulphate, sodium, and chloride concentrations, He-excess, CFC-11 concentration and tritium content for selected wells located upstream and downstream from the fault. See text for discussion

 DOI 10.1007/s10040-014-1188-z

is in the form of $^{3}He_{trit}$ attributed to the decay of tritium (Fig. 8). Therefore, isotope data support borehole and chemical data; chemical anomalies together with helium excesses, low CFC and tritium concentrations point out the existence of a deep buried fault. This mixing scheme provides a plausible explanation as to the source of poor pre-mining groundwater quality downstream from the fault line in the shallow aquifer system that sustains the Ova Stream.

Summary and conclusions

This study defines the isotopic features of the three aquifers located above the trona deposit in the Kazan Basin in Central Anatolia. The groundwater residence times in these aquifers were estimated by using isotope data. The $\delta^{18}O$ and δD data show a strong isotopic contrast between the shallow and deeper aquifer systems and even between the unconfined and confined parts of the middle and deep aquifers. There is nearly −3 ‰ depletion in $\delta^{18}O$ values and −25 ‰ in δD values from shallow to deep groundwater systems and it is not possible to explain this depletion solely with the recharge elevation of the deep aquifer being higher than the shallow aquifer.

Chlorofluorocarbon (CFC-11 and CFC-12) concentrations and tritium contents are high in the shallow aquifer system, indicating modern recharge, except for three samples: S-4, S-9 and S-11 with concentrations close to the detection limit. This finding shows that there is mixing of deeper, old groundwater in those wells, most likely along the NE–SW striking fault. The CFC based recharge years range from 1963 to 1987 for the shallow aquifer system. It is only possible to calculate $^{3}H/^{3}He_{trit}$ ages of a few samples because of addition of older groundwater with high terrigenic He concentrations. These ages are quite different from the CFC-ages, but the differences can be explained by mixing.

The ^{13}C mixing method was utilized to correct the radiocarbon ages affected by an extensive water rock interaction as indicated by $\delta^{13}C$ data. The estimated radiocarbon ages came out to be modern for the samples from the shallow system and up to 34 ka BP in the middle and deep aquifer systems.

Analysis of helium isotope components shows that mantle-He is most prominent in groundwater from a shallow well, S-11, most likely originating in a deep, buried fault. The existence of this fault brings water from the deeper parts to the shallow wells S-3, S-4, S-9 and S-11. Therefore, the existence of such connections between the deep and shallow aquifers may adversely affect the groundwater quality of the shallow aquifer downstream from the buried fault. Thus, the presence of the buried fault striking in NE–SW direction is an important structural feature that may have a significant control on the dynamics of the groundwater flow and the mixing mechanisms with significant effect on the groundwater quality of the shallow system. This information would be of significant value in analyzing the impacts of solution mining on the groundwater quality of the shallow aquifer system. Thus, the existing hydrogeological conceptual model of the site should be updated with the information generated in this study and the numerical groundwater model should be revised accordingly. Finally, it is concluded that while hydraulic and hydrochemical data may be sufficient to develop conceptual models for simple systems, they should be augmented with the data obtained from environmental tracers and noble gases for systems having complex flow dynamics and mixing mechanisms.

Acknowledgements Part of this study was supported by The Scientific and Technological Research Council of Turkey Environmental, Atmospheric, Earth and Marine Sciences Research Group (CAYDAG) Short-Term R&D Funding Program (1002) Project No. 106Y310. Sebnem Arslan was supported by the fellowship of Fulbright Commission of Turkey during her research at Lamont-Doherty Earth Observatory of Columbia University. The authors would like to thank Eugene Gorman for valuable assistances during CFC measurements, and Mehmet Ekmekci and Nilgun Gulec for their advice. The assistance of Faruk Suluki, Omer Kahraman, Ugur Ozturk and Lutfu Simsek in the field are appreciated. Special thanks to Riotur Mining Inc. for giving access to the hydrogeologic and hydrochemical data. The manuscript was considerably improved by constructive criticism and comments provided by reviewers, including C. Kohfahl, M. Currell and J. Führböter.

References

Aeschbach-Hertig W, Schlosser P, Stute M, Simpson HJ, Ludin A, Clark JF (1998) A $^{3}H/^{3}He$ study of ground water flow in a fractured bedrock aquifer. Ground Water 36:661–670

Aeschbach-Hertig W, Peeters F, Beyerle U, Kipfer R (2000) Palaeotemperature reconstruction from noble gases in ground water taking into account equilibration with entrapped air. Nature 405:1040–1044

Apaydin A (2004) Study of recharge and conditions of Cakiloba-Karadoruk aquifer system (western Beypazari-Ankara). PhD Thesis, Hacettepe University, Turkey

Arslan S (2008) Investigation of the recharge and discharge mechanisms of a complex aquifer system by using environmental isotopes and noble gases. PhD Thesis, Middle East Technical University, Turkey

Arslan S, Yazicigil H, Stute M, Schlosser P (2013) Environmental isotopes and noble gases in the deep aquifer system of Kazan Trona Ore Field, Ankara, central Turkey and links to paleoclimate. Quat Res 79:292–303

ASTM (1999) Standard test methods for low-level dissolved oxygen in water. D5543-94, ASTM, West Conshohocken, PA

Bayari CS, Ozyurt NN, Kilani S (2009) Radiocarbon age distribution of groundwater in the Konya Closed Basin, Central Anatolia, Turkey. Hydrogeol J 17:347–365

Bethke MC, Johnson TM (2008) Groundwater age and groundwater age dating. Annu Rev Earth Planet Sci 36:121–152

Bottema S, van Zeist W (1981) Palynological evidence for the climatic history of the near East, 50,000–6,000 BP. Paper presented at the Prehistoire du Levant, Paris, 1981, CNRS, Paris

Bullister JL (2011) Atmospheric CFC-11, CFC-12, CFC-113, CCl4 and SF6 histories. Carbon Dioxide Information Analysis Center, Oak Ridge National Laboratory, US DOE, Oak Ridge, TN. doi:10.3334/CDIAC/otg.CFC_Hist. Available at http://cdiac.ornl.gov/ftp/oceans/CFC_ATM_Hist/. Accessed 15 Dec 2013

Busenberg E, Plummer LN (1992) Use of chlorofluorocarbons (CCl_3F and CCl_2F_2) as hydrologic tracers and age-dating tools:

the alluvium and terrace system of central Oklahoma. Water Resour Res 28:2257–2283
Busenberg E, Plummer LN (2000) Dating young groundwater with sulfur hexafluoride: natural and anthropogenic sources of sulfur hexafluoride. Water Resour Res 36:3011–3030
Camur MZ, Er C, Yazicigil H (2008) Modeling of lithology induced chemical anomalies in the aquifer systems of the Kazan Trona deposit area, Ankara, Turkey. Environ Geol 54:777–789
Castro MC, Stute M, Schlosser P (2000) Comparison of ^{4}He ages and ^{14}C ages in simple aquifer systems: implications for groundwater flow and chronologies. Appl Geochem 15:1137–1167
Cetin B, Unc E, Uyar G (2002) The moss flora of Ankara-Kizilcahamam-Camkoru and Camlidere districts. Turk J Bot 26:91–101
Clark I, Fritz P (1997) Environmental isotopes in hydrogeology. CRC, Boca Raton, FL
Clark JF, Stute M, Schlosser P, Drenkard S (1997) A tracer study of the Floridan aquifer in southeastern Georgia: implications for groundwater flow and paleoclimate. Water Resour Res 33:281–289
Clarke WB, Jenkins WJ, Top Z (1976) Determination of tritium by mass-spectrometric measurement of ^{3}He. Int J App Radiat Isot 27:515–522
Cook PG, Favreau G, Dighton JC, Tickell S (2003) Determining natural groundwater influx to a tropical river using radon, chlorofluorocarbons and ionic environmental tracers. J Hydrol 277:74–88
Craig H (1961) Isotopic variations in meteoric waters. Science 133:1702–1703
Drimmie RJ, Shouakar-Stash O, Walters R, Heemskerk AR (2001) Hydrogen isotope ratio by automatic, continuous flow, elemental analyses, and isotope ratio mass spectrometry. University of Waterloo, Waterloo, ON, 8 pp
DSI (1975) Ankara-Murted Plain hydrogeological investigation report. General Directorate of State Hydraulic Works (DSI), Ankara, 49 pp
Dunkle SA, Plummer LN, Busenberg E, Phillips PJ, Denver J, Hamilton PA, Michel RL, Coplen TB (1993) Chlorofluorocarbons (CCl_3F and CCl_2F_2) as dating tools and hydrologic tracers in shallow groundwater of the Delmarva Peninsula, Atlantic Coastal-Plain, United States. Water Resour Res 29:3837–3860
Eberts SM, Böhlke JK, Kauffmann J, Jurgens BC (2012) Comparison of particle-tracking and lumped-parameter age distribution models for evaluating vulnerability of production wells to contamination. Hydrogeol J 20:263–282
Epstein S, Mayeda T (1953) Variation of O^{18} content of waters from natural sources. Geochim Cosmochim Acta 4:213–224
Gilbert TW, Behymer TD, Castaneda HB (1982) Determination of dissolved-oxygen in natural and wastewaters. Am Lab 14:119–134
Global Network of Isotopes in Precipitation (2006) The GNIP database. Available at http://www-naweb.iaea.org/napc/ih/IHS_resources_gnip.html. Accessed 15 Dec 2013
Jenkins WJ, Clarke WB (1976) Distribution of ^{3}He in western Atlantic Ocean. Deep-Sea Res 23:481–494
Kazanci N, Gokten E (1988) Lithofacies features and tectonic environment of the continental Paleocene volcanoclastics in Ankara region. METU J Pure Appl Sci 21:271–282
Kocyigit A, Lunel AT (1987) Geology and tectonic setting of Alci region, Ankara. METU J Pure Appl Sci 20:35–57
Kocyigit A, Ozkan S, Rojay B (1988) Examples from fore-arc basin remnants of the active margin of northern Neo-Tethys: development and emplacement ages of the Anatolian Nappes, Turkey. METU J Pure Appl Sci 21:183–210
Kulongoski JT, Hilton DR, Izbicki JA (2003) Helium isotope studies in the Mojave Desert, California: implications for groundwater chronology and regional seismicity. Chem Geol 202:95–113
Ludin A, Weppernig R, Boenisch G, Schlosser P (1998) Mass spectrometric measurement of helium isotopes and tritium. Lamont-Doherty Earth Observatory, New York
Mamyrin BA, Tolstikhin IN (1984) Helium isotopes in nature. Elsevier, Amsterdam
Martel DJ, Deak J, Dovenyi P, Horvath F, Onions RK, Oxburgh ER, Stegena L, Stute M (1989) Leakage of helium from the Pannonian Basin. Nature 342:908–912
Marty B, Torgersen T, Meynier V, Onions RK, Demarsily G (1993) Helium isotope fluxes and groundwater ages in the Dogger Aquifer, Paris Basin. Water Resour Res 29:1025–1035
Newman BD, Osenbrück K, Aeschbach-Hertig W, Solomon DK, Cook P, Różański K, Kipfer R (2010) Dating of 'young' groundwaters using environmental tracers: advantages, applications, and research needs. Isot Environ Health Stud 46:259–278
Pearson FJ (1965) Use of $^{13}C/^{12}C$ ratios to correct radiocarbon ages of material initially diluted by Limestone. 6th Int. Conf. on Radiocarbon and Tritium Dating, Pullman, WA, June 1865, 357 pp
Pearson FJ, Hanshaw BB (1970) Sources of dissolved carbonate species in groundwater and their effects on Carbon-14 dating. Paper presented at the Symp. on Isotope Hydrology, Vienna, March 1970
Plummer LN, Busenberg E (2000) Chlorofluorocarbons. In: Cook PG, Herczeg AL (eds) Environmental tracers in subsurface hydrology. Kluwer, Dordrecht, The Netherlands
Plummer LN, Busenberg E, Han LF (2006) Data interpretation in representative cases. In: Use of chlorofluorocarbons in hydrology: a guidebook, chap 8. IAEA, Vienna, pp 105–134
Poreda RJ, Cerling TE, Salomon DK (1988) Tritium and helium isotopes as hydrologic tracers in a shallow unconfined aquifer. J Hydrol 103:1–9
Prentice IC, Guiot J, Harrison SP (1992) Mediterranean vegetation, lake levels and paleoclimate at the last glacial maximum. Nature 360:658–660
Robertson WD, Cherry JA (1989) Tritium as an indicator of recharge and dispersion in a groundwater system in central Ontario. Water Resour Res 25:1097–1109
Rojay B, Toprak V, Bozkurt E (2002) Core sample analysis in Kazan Soda Project Area. Middle East Technical University, Ankara
Samborska K, Rózkowski A, Maloszewski P (2013) Estimation of groundwater residence time using environmental isotopes (14C, T) in carbonate aquifers, southern Poland. Isot Environ Health Stud 49:73–97
Sanford W (2011) Calibration of models using groundwater age. Hydrogeol J 19:13–16
Schlosser P, Stute M, Dorr H, Sonntag C, Munnich KO (1988) Tritium/^{3}He dating of shallow groundwater. Earth Planet Sci Lett 89:353–362
Schlosser P, Stute M, Sonntag C, Munnich KO (1989) Tritiogenic ^{3}He in shallow groundwater. Earth Planet Sci Lett 94:245–256
Shapiro SD, Schlosser P, Smethie WM, Stute M (1997) The use of ^{3}H and tritiogenic ^{3}He to determine CFC degradation and vertical mixing rates in Framvaren Fjord, Norway. Mar Chem 59:141–157
Smethie WM, Fine RA, Putzka A, Jones EP (2000) Tracing the flow of North Atlantic Deep Water using chlorofluorocarbons. J Geophys Res Oceans 105:14297–14323
Solomon DK, Sudicky EA (1991) Tritium and ^{3}He isotope ratios for direct estimation of spatial variations in groundwater recharge. Water Resour Res 27:2309–2319
Solomon DK, Genereux DP, Plummer LN, Busenberg E (2010) Testing mixing models of old and young groundwater in a tropical lowland rain forest with environmental tracers. Water Resour Res 46, W04518
SRK (2001) Hydrogeology: conceptual understanding. Kazan Trona Project report, Ankara, Turkey
SRK (2003) Water supply assessment. Kazan Trona Project report, Ankara, Turkey
SRK (2004) Hydrogeological modeling. Kazan Trona Project report, Ankara, Turkey
Stute M, Deak J (1989) Environmental isotope study (^{14}C, ^{13}C, ^{18}O, D, noble gases) on deep groundwater circulation systems in Hungary with reference to paleoclimate. Radiocarbon 31:902–918
Stute M, Schlosser P, Clark JF, Broecker WS (1992a) Paleotemperatures in the southwestern United States derived from noble gases in ground water. Science 256:1000–1003

 DOI 10.1007/s10040-014-1188-z

Stute M, Sonntag C, Deak J, Schlosser P (1992b) Helium in deep circulating groundwater in the Great Hungarian Plain: flow dynamics and crustal and mantle helium fluxes. Geochim Cosmochim Acta 56:2051–2067

Stute M, Forster M, Frischkorn H, Serejo A, Clark JF, Schlosser P, Broecker WS, Bonani G (1995) Cooling of tropical Brazil (5-degrees-C) during the last glacial maximum. Science 269:379–383

Stute M, Deak J, Revesz K, Bohlke JK, Deseo E, Weppernig R, Schlosser P (1997) Tritium/^{3}He dating of river infiltration: an example from the Danube in the Szigetkoz area, Hungary. Ground Water 35:905–911

Szabo Z, Rice DE, Plummer LN, Busenberg E, Drenkard S (1996) Age dating of shallow groundwater with chlorofluorocarbons, tritium helium 3, and flow path analysis, southern New Jersey coastal plain. Water Resour Res 32:1023–1038

Toprak V, Rojay B (2000) Geology baseline study for the Kazan Soda Project Area. Middle East Technical University, Ankara

Toprak V, Rojay B (2001) Geological investigation in Kazan Soda Project Area. Middle East Technical University, Ankara

Torgersen T, Stute M (2013) Helium (and other noble gases) as a tool for understanding long time-scale groundwater transport. In: Isotope methods for dating old groundwater, IAEA, Vienna, pp 179–216

US Geological Survey (2011) The Reston Chlorofluorocarbon Laboratory, US Geological Survey, Reston, VA. http://water.usgs.gov/lab/. Accessed 15 Dec 2013

Varni M, Carrera J (1998) Simulation of groundwater age distributions. Water Resour Res 34:3271–3281

Warner MJ, Weiss RF (1985) Solubilities of chlorofluorocarbon-11 and chlorofluorocarbon-12 in water and seawater. Deep-Sea Res 32:1485–1497

Weise SM (1986) Heliumisotopen: Gehalte im Grundwasser—Messung und Interpretation [Helium isotopes: contents in groundwater—measurements and interpretation]. PhD Thesis, University of München, Germany

Weise SM, Moser H (1987) Groundwater dating with helium isotopes. In: Techniques in water resources development, IAEA, Vienna, pp 105–126

Weiss RF (1968) Piggyback samplers for dissolved gas studies on sealed water samples. Deep-Sea Res 15:695–699

Weissmann GS, Zhang Y, LaBolle EM, Fogg GE (2002) Dispersion of groundwater age in an alluvial aquifer system. Water Resour Res 38(10):1198

Wick L, Lemcke G, Sturm M (2003) Evidence of Lateglacial and Holocene climatic change and human impact in eastern Anatolia: high-resolution pollen, charcoal, isotopic and geochemical records from the laminated sediments of Lake Van, Turkey. The Holocene 13:665–675

Woods Hole Oceanographic Institution (2011) NOSAMS, National Ocean Sciences Accelerator Mass Spectrometry Facility. http://www.whoi.edu/nosams/. Accessed 08 Aug 2014

Yager RM, Plummer LN, Kauffman LJ, Doctor DH, Nelms DL, Schlosser P (2013) Comparison of age distributions estimated from environmental tracers by using binary-dilution and numerical models of fractured and folded karst: Shenandoah Valley of Virginia and West Virginia, USA. Hydrogeol J 21:1193–1217

Yazicigil H, Doyuran V, Camur MZ, Duru U, Sakiyan J, Yilmaz KK, Toprak FO, Pusatli T (2001) Hydrogeological–hydrogeochemical baseline study of the Kazan Trona Project Area. Middle East Technical University, Ankara, 355 pp

Yazicigil H, Er C, Ates JS, Camur MZ (2009) Effects of solution mining on groundwater quality in the Kazan Trona Field, Ankara-Turkey: model predictions. Environ Geol 57:157–172